Pérez-Consuegra, N., Ott, R. F., Hoke, G. D., Galve, J. P., Pérez-Peña, V., Mora, A. (2021): Neogene variations in slab geometry drive topographic change and drainage reorganization in the Northern Andes of Colombia. - Global and Planetary Change, 206, 103641.

https://doi.org/10.1016/j.gloplacha.2021.103641

Manuscript revised and resubmitted to: Global Planetary Change (Special Issue)

Neogene variations in slab geometry drive topographic change and drainage reorganization in the Northern Andes of Colombia

Nicolás Pérez-Consuegra[1*], Richard F. Ott[2], Gregory D. Hoke[1], Jorge P. Galve[3], Vicente Pérez-Peña[3], Andrés Mora[4]

1. Department of Earth and Environmental Sciences, Syracuse University. Syracuse, USA

2. German Centre for Geoscience Research, Potsdam, Germany

3. Departamento de Geodinámica, Universidad de Granada. Granada, Spain

4. Ecopetrol Brazil, Rio de Janeiro, Brazil

*Corresponding author. Email: nperezco@syr.edu

Abstract

The tropical Northern Andes of Colombia are one the world's most biodiverse places, offering an ideal location for unraveling the linkages between the geodynamic forces that build topography and the evolution of the biota that inhabit it. In this study, we utilize geomorphic analysis to characterize the topography of the Western and Central Cordilleras of the Northern Andes to identify what drives landscape evolution in the region. We supplement our topographic analysis with erosion rate estimates based on gauged suspended sediment loads and river incision rates from volcanic sequences. In the northern Central Cordillera, an elevated low-relief surface (2,500 m in elevation, ~40 x 110 km in size) with quasi-uniform lithology and surrounded by knickpoints, indicates a recent increase in rock and surface uplift rate. Whereas the southern segment of the Central Cordillera shows substantially higher local relief and mostly well graded river profiles consistent with longer term uplift-rate stability. We also identify several areas of major drainage reorganization, including captures and divide migrations. These changes in the topography coincide with the proposed location of a slab tear and flat slab subduction under the northern Central Cordillera, as well as with a major transition in the channel slope of the Cauca River. We identify slab flattening as the most likely cause of strong and recent uplift in the Northern Andes leading to ~2 km of surface uplift since 8–4 Ma. Large scale drainage reorganization of major rivers is likely driven by changes in upper plate deformation in relation to development of the flat slab subduction geometry; however, south of the slab tear other factors, such as emplacement of volcanic rocks, also play an important role. Several biologic observations above the area of slab flattening suggest that surface uplift isolated former lowland species on the high elevation plateaus, and drainage reorganization may have influenced the distribution of aquatic species.

Keywords

drainage reorganization, uplift, knickpoint migration, tropics, biodiversity

1. Introduction

Since Alexander von Humboldt's work on the Chimborazo volcano, the Northern Andes of South America have been noted as one of Earth's most biodiverse regions (Rahbek et al., 2019; von Humboldt and Bonpland, 2013). Many studies have shown that topography and its evolution through time are important predictors of modern-day biodiversity globally, and especially within the Northern Andes (Antonelli et al., 2018; Antonelli and Sanmartín, 2011; Badgley et al., 2017). Therefore, a clear understanding of the timing and spatial patterns of topographic growth is necessary to discern the generation of the observed modern biodiversity patterns in the Andes (Baker et al., 2014; Hoorn et al., 2010; Luebert and Weigend, 2014), but is also critical to identifying the tectonic, geodynamic and climatic processes that generate topography (Garzione et al., 2017; Horton, 2018; Schildgen and Hoke, 2018). The Northern Andes of Colombia are a region of complex topography above the Nazca subduction zone, with three roughly north-south striking parallel mountain chains separated by intermontane basins. The regional topography is overall controlled by subduction processes, yet we know little about the topographic growth especially of the Western and Central Cordillera. A change in subduction geometry from steep to shallow beginning around 6–8 Ma has been proposed, which is expected to have a significant effect on topography (e.g., Eakin et al., 2014) and by extension, an imprint in modern biodiversity. However, the topographic evolution of the Western and Central Cordillera remains elusive, as do the contributions of different drivers of topographic change such as subduction geometry and drainage reorganization.

Extensive geochronology and geochemistry of rocks in the Central and Western Cordillera have been used to decipher the Mesozoic and Cenozoic evolution of the magmatism and terrane accretion events (Kerr et al., 1998, 1997; Villagómez et al., 2011). Specifically, thermochronology, a method that records the cooling of rocks as they are advected towards the surface via the removal of overlying rocks, termed exhumation (Malusà and Fitzgerald, 2019; Reiners and Brandon, 2006), has been applied to identify periods of mountain building. Thermochronology data from the Central Cordillera generally point towards high rates of exhumation in the Late Cretaceous to Paleogene between ~50–70 Ma, related to the accretion of oceanic terranes (Villagómez et al., 2011; Zapata et al., 2020). The Western Cordillera shows a pulse of exhumation at ~40 Ma followed by a decrease in rates (Villagómez and Spikings, 2013). Few data exist to constrain the

Neogene topographic evolution of the Western and Central Cordilleras of the Northern Andes remains poorly understood (e.g., Mora et al., 2019).

The main Neogene tectonic events are the collision of the Panama Block during the Middle Miocene (ca. 12–15 Ma) with South America (Farris et al., 2011; Montes et al., 2015, 2012) followed by tearing of the Nazca slab at ca. 6–8 Ma and subsequent initiation of flat slab subduction north of ~5°N (Fig. 1A; Chiarabba et al., 2016; Vargas and Mann, 2013; Wagner et al., 2017). Thermal history models from apatite fission track data in the Western and Central Cordilleras show higher rates of exhumation south of the slab tear over the past 40 Ma (Villagómez and Spikings, 2013). Lower temperature apatite (U-Th)/He (AHe) ages of the Central Cordillera, which record exhumation from ~2–3 km in the crust, are younger south of the slab tear, indicating higher exhumation compared to the north.

The cause of the differences in thermochronology ages, and the general effects of the transition from normal to flat slab on the Western and Central Cordilleras' topography remain elusive. Flat slab subduction is generally associated with changes in the rates of patterns of strain in the upper plate while also inducing dynamic vertical motions (Dávila and Lithgow-Bertelloni, 2013; Espurt et al., 2008; Gutscher et al., 2000; Horton, 2018; Martinod et al., 2020). Several studies, advocate for increased crustal shortening and rock uplift above the zone of flat slab subduction due to increased coupling between the upper and lower plates (Espurt et al., 2008; Gutscher et al., 2000) or isostatic adjustment (Eakin et al., 2014), yet thermochronological data record more and faster exhumation in the southern steeper slab segment (Villagómez and Spikings, 2013). The rate dependent integration time of the employed thermochronometry may be too long to capture a recent increase in uplift rates in the north in response to slab flattening. Such changes in subduction dynamics and tectonic uplift rates may also induce drainage reorganization. Yet, there is no data on past and present rates of modern drainage reorganization within the Central and Western Cordillera.

In this paper, we use geomorphic tools to characterize the topography of the Western and Central Cordilleras of the Northern Andes (Colombia), identify areas and mechanisms of drainage reorganization, and discuss the roles of tectonic events such as slab flattening, Panama Block collision and volcanism in the topographic evolution of the region. Our analysis combines simple topographic observations through swath profiles and detailed analyses of the river network. We employ the analysis of river long profiles to map knickpoints (kinks in river profiles) that can be related to temporal changes in tectonic uplift rates (e.g., Wobus et al., 2006), and river steepness to elucidate spatial patterns of uplift and erosion rates. We also investigate metrics that indicate drainage reorganization, e.g., the χ-index to map the stability of drainage basins (Forte and Whipple, 2018; Scherler and Schwanghart, 2020; Willett et al., 2014). We integrate our topographic observations with geological data, climatic data and erosion rate estimates based on gauged suspended sediment loads. The topographic features we identify indicate a dynamic landscape that is responding to spatial and temporal changes in rock uplift and drainage reorganization. Our observations help identify the potential drivers of topographic change and highlight linkages between landscape evolution and the modern distribution of species.

2. Geology of the Western and Central Cordillera

The Northern Andes are bounded to the west by the Nazca subduction trench and the Panama Block, by the South Caribbean Deformed Belt to the north, and the East Andean Fault System to the east (e.g., Pennington, 1981). The Nazca Plate subducts below South America at a rate of ~5 cm/yr (e.g., Trenkamp et al., 2002). In the Middle Miocene (ca. 12–15 Ma), the Panama

Block collided with northwest South America producing rock uplift and closure of the Central American Seaway (Farris et al., 2011; León et al., 2018; Montes et al., 2015, 2012). The spatial and temporal patterns in the distribution of volcanism from the Miocene to the present have been used to reconstruct the evolution of the slab geometry and the onset of flat slab subduction at ~6–8 Ma (Wagner et al., 2017).

The Northern Andes comprise three roughly north striking mountain ranges—the Western, Central and Eastern Cordilleras separated by the Cauca and Magdalena intermontane basins (Fig. 1B). The Central Cordillera is composed of pre-Mesozoic, low- to high-grade metamorphic basement of mixed continental and oceanic origin that is intruded by numerous Mesozoic–Cenozoic plutons of the Andean magmatic arc (Aspden et al., 1987; Aspden and McCourt, 1986; Cediel et al., 2005). In its southern segment, the eastern flank of the Central Cordillera is bounded by the Plata-Chusma Fault (reverse). On its northern segment the Central Cordillera forms an east-dipping basement that is buried beneath the Middle Magdalena Valley Basin (Gómez et al., 2005, 2003). The Miocene to present slip rates of the east-bounding fault of the northern Central Cordillera are likely lower compared to the slip rates on the west bounding Romeral Fault zone (e.g., Gomez et al., 2003). The Cauca-Romeral Fault is a west-vergent thrust fault system with varying strike-slip motion that marks the boundary between the Western and Central Cordilleras (Fig. 1B). At ~700 km in length, the Cauca-Romeral fault is one of the most continuous active fault systems in Colombia. The kinematics of the fault change along its course from reverse sinistral to reverse dextral somewhere around 5°N (Ego et al., 1995; Paris et al., 2000; Veloza et al., 2012). The Cauca–Romeral Fault thrusts metamorphic basement of the Central Cordillera and Cretaceous ophiolitic basement over the Cenozoic deposits of the Cauca Basin (e.g., Alfonso et al., 1994).

The Western Cordillera is mainly composed of Cretaceous volcanic and sedimentary rocks of oceanic affinity that were accreted to the continental margin of the Central Cordillera during the Paleogene along the suture that comprises the Cauca-Romeral Fault (e.g., Kerr et al., 1997; Kerr and Tarney, 2005; Fig. 1B). The Western Cordillera is bounded to the west by the Uramita Fault Zone, a major suture zone with a dextral transpressional regime (e.g., Duque-Caro, 1990; León et al., 2018; Trenkamp et al., 2002).

The basement of the intermontane Cauca Basin, between the Western and Central Cordillera, is composed of the same Cretaceous ophiolitic rocks of the Western Cordillera, unconformably overlain by up to ~4 km of Paleocene to middle Miocene marine and continental sedimentary rocks (e.g., Alfonso et al., 1994), which in turn are unconformably overlain by late Miocene to Holocene alluvial and lacustrine sediments. Shallow marine to intertidal rocks of the Esmita Formation in the southern Cauca and Patía Basins (Gallego–Ríos et al., 2020; A Murcia and Cepeda, 1991) show that, at least until the early Miocene, these areas lied at sea level and imply that the Western Cordillera had yet to fully form. The late Miocene to Holocene sedimentary rocks are locally deformed with both syn- and post-depositional faulting related to the transpressional regime of this part of the Colombian Andes (Neuwerth et al., 2006; Suter et al., 2008). The Patía intermontane basin (Fig. 1) also consists of Cretaceous ophiolitic basement unconformably overlain by deformed Paleocene–Miocene rocks (Gallego–Ríos et al., 2020), followed by an unconformity covered by flat lying Pliocene to Quaternary volcanic and volcaniclastic rocks (Echeverri et al., 2015; Gallego–Ríos et al., 2020; A Murcia and Cepeda, 1991).

3. Methods

3.1 Topographic and river network analyses

We analyzed the spatial variations in topography in the Western and Central Cordillera of the Northern Andes by calculating different geomorphic metrics using Topotoolbox (Schwanghart and Scherler, 2014) and the 90 m GLO-90 digital elevation model (DEM) from the European Space Agency (https://spacedata.copernicus.eu), together with Geographic Information Systems (GIS software) for graphical display. Topographic metrics calculated from the DEM include local relief, hillslope gradient and swath profiles.

Local relief was calculated from the difference between the minimum and maximum elevations within a 0.5 km and 1-km radius. Hillslope gradient was calculated as the rise over run change in elevation across cells of the DEM using the gradient8 function in TopoToolbox. Swath profiles are cross-sections of topography calculated by averaging data along a rectangle of prescribed width.

River networks in active mountain ranges can record temporal and spatial patterns in tectonics and climatic (e.g., Wobus et al., 2006). Therefore, we calculated the normalized channel steepness index (k_{sn}) (Whipple and Tucker, 1999), and χ (Perron and Royden, 2013) as well as river elevation versus χ-profiles. k_{sn} and χ were calculated using the standard TopoToolbox functions with quantile carving (tau=0.5) applied to smooth the stream network. The evolution of a river profile is commonly described by the stream power incision model (Howard, 1994):

$$(1)\ \frac{dz}{dt} = U - E = U - K * A^m * S^n$$

where U is the rock uplift rate, E erosion rate, A drainage area, S the local channel slope, m and n empirical scaling factors, and K a dimensional coefficient that incorporates the effects of lithology, climate, incision process and hydrology (e.g., Whipple and Tucker, 1999). Rivers will tend to balance the amount of rock uplift by erosion to achieve a steady state profile over time ($dz/dt = 0$). In this case, the local steady state channel slope can be expressed as

$$(2)\ \boldsymbol{S = k_s * A^{-\theta}}$$

with $k_s = (U/K)^{1/n}$ and $\theta = m/n$, where k_s is the channel steepness corrected for drainage area (Flint, 1974). θ is the river profile concavity and often fixed to a reference value (θ_{ref}) to calculate the normalized channel steepness, which allows the comparison of rivers within a region (e.g., Wobus et al., 2006):

$$(3)\ \boldsymbol{S = k_{sn} * A^{-\theta_{ref}}}$$

k_{sn} can now be used to infer differences in rock uplift rates of steady state rivers within regions of constant or similar K, e.g., regions of similar lithology and climate. The values of k_{sn} and concavity can be estimated by logarithmic regression of channel slope and drainage area data. However, this analysis can be noisy and Perron and Royden (2013) introduced the χ-integral method to make this analysis more robust. Assuming spatially invariant U and K equation (5) can be integrated to

$$(4)\ \boldsymbol{z(x) = z(x_b) * \left(\frac{U}{K * A_0^m}\right)^{1/n} * \chi}$$

where $\chi = \int_{x_b}^{x} {A_0/A}^{\theta_{ref}}$, x_b is the base level for integration, A_0 an arbitrary scaling area, and χ the horizontal transformation of the distance along the river. We used a common baselevel of 250 m for the integration, which corresponds to the approximate elevation where the Cauca and Patia rivers flow from the Northern Andes onto their alluvial plains. It is important to notice that the slope of χ versus elevation plots is equivalent to the channel steepness k_{sn}, if A_0 is assumed to be 1. Therefore, χ-elevation plots are a simple way of assessing the steepness of a river and its potential variations along its profile. Furthermore, differences of χ-values across drainage divides can indicate differences in river steepness and basin geometry and therefore predict the migration of drainage divides (for more details see e.g., Willett et al., 2014).

We find our best-fit river channel concavity of the region with a Bayesian optimization algorithm. Steady state river profiles should exhibit a straight line in χ-elevation plots (Royden and Perron, 2013). We clip DEMs of the Western and Central Cordillera to the fronts of the mountain ranges to avoid alluviated foreland rivers and use a TopoToolbox algorithm (mnoptim) for the optimization. The algorithm selects random subsets of the river network and finds the concavity that best linearizes the χ-elevation profiles of the region. We find a best fit of $\theta_{ref} = 0.5$ both in the Western and Central Cordillera (Fig. S1) and use this value for all subsequent calculations of k_{sn} and χ.

Knickpoints or short channel segments where channel steepness increases abruptly can be indicative of temporal changes in uplift rate (e.g., Wobus et al., 2006). To identify regions where uplift rates may have recently changed, in an objective manner, we use a knickpoint-search algorithm (Schwanghart and Scherler, 2014). The algorithm identifies (upward) convexities in river profiles, by measuring the offset between the actual river profile and a strictly concave projection. A knickpoint is identified if the difference between the actual and projected profile exceeds a tolerance value of 200 m.

We utilize *DivideTools* (Forte and Whipple, 2018) to calculate drainage divide stability metrics averaged upstream of a reference drainage area ($10^7 m^2$) for selected basins across major drainage divides. We employ across-divide differences in mean gradient, mean local relief and χ.

3.2 Climate data

We use remotely sensed precipitation to explore how climate may influence topography. Mean annual precipitation (MAP) data are taken from the CHELSA database with 1 km resolution (Fig. S2; Karger et al., 2017). We acknowledge that historical precipitation datasets are imperfect for comparison with geomorphic data because these products characterize precipitation over the past few decades while the landscapes evolve on 10^3–10^6 years timescales (Hack, 1960). Nevertheless, we use the historical climate data as a first order estimate.

3.3 Decadal erosion rates

We calculate decadal erosion rates from suspended load and water discharge data (e.g., Carretier et al., 2018) from three hydrological stations in the Cauca and Patía catchments (Table S1) managed by the Instituto de Hidrología, Meteorología y Estudios Ambientales (IDEAM, Colombia). In the Cauca, stations are located at the northern termination of the Upper Cauca Valley and downstream of the mouth of the Cauca Canyon, where the Cauca enters the plain of the Lower Magdalena Valley Basin. Another station is located at the outlet of the Upper Patía Valley at the eastern margin of the Western Cordillera.

We fit a power-law to sediment load versus fluvial discharge or stage data which consists of 8–16 observations per location (Fig. S3). We then apply this power-law fit to the complete record of daily discharge to estimate sediment load over the full gauging period of ~20–60 years depending on location (Fig. S4). We converted sediment load data to catchment average erosion rates by determining catchment area and assuming an initial rock density of 2600kg/m^3. The sediment load data for the Patia River was obtained in [Kton/yr] from Figure 6b from Restrepo and Kjerfve (2002). We report the mean and standard deviation of the annual sediment load data and show the distributions in Fig. S4.

4. Results

4.1 Topography north and south of the slab tear

The E-W swath profiles across the Central Cordillera (Fig. 2A,B) show that north of the slab tear the topography forms a low-relief plateau about 40 km wide and at ~2,500 m elevation, the Antioqueño Plateau (AP). Local relief on this plateau is less than 200 m (Fig. 2). At its eastern margin, the AP transitions into a ~70 km long east sloping surface of similarly low relief that is in parts dissected by up to 900 m deep river canyons, before plunging into the Magdalena River Valley.

South of the slab tear, the E-W swath profile across the Central Cordillera reveals a more symmetrical, triangular mountain range (Fig. 2C). Increased variance in topography indicates substantially higher local relief of ~ 700 m compared to the northern Central Cordillera. The N-S swath profile along the crest of the Central Cordillera shows the same pattern, where north of the slab tear the landscape forms a low-relief, high elevation region dissected by deep river valleys, and south of the slab tear relief increases substantially.

4.2 River network analysis: k_{sn}, χ and river profiles

The drainage network metrics show differences north and south of the slab tear, reinforcing the patterns observed in the basic topographic observations (Figure 3). North of the slab tear, channel steepness is low in the low-relief surfaces around the Antioqueño Plateau and higher along the margins of the Central Cordillera. To the south, channel steepness is generally high in the Central Cordillera and low in the intermontane Cauca Basin.

North of the slab tear, χ maps show contrasting χ values between the catchments draining large portions of the low-relief surfaces (high χ values) and the catchments draining the steep margins of the western flank of the Central Cordillera into the Cauca River (low χ values). This suggests that drainage divide migration is occurring and the steep catchments draining the western flank of the Central Cordillera are capturing area from the catchments draining the low-relief surfaces of the Antioqueño Plateau. Across–divide χ-values can be biased by differences in uplift rate, therefore we also compared other topographic metrics indicative of divide migration. The across–divide differences in hillslope gradient and local relief document higher relief and gradient on the divide side with lower χ value (western flank of Central Cordillera) and are consistent with the divide motion predicted by the χ-values (Figs. 3A and 4A). South of the slab tear, a large contrast in χ appears between the headwaters of the Cauca and Patía rivers (Figs. 3A and 4B). Values of χ are higher in the headwaters of the Cauca Basin. This pattern in χ suggests that drainage divide migration is occurring and the steep Patía Basin is capturing area from the upper segment of the Cauca River Basin. This is also reflected in the channel steepness values and hillslope gradient across the drainage divide of the upper Patía and Cauca River basins, with higher values in the Patía River Basin. Rivers draining the western flank of the Western Cordillera also have a marked difference in χ with respect to the rivers draining the eastern flank into the Cauca Basin. Rivers draining the western flank of the Western Cordillera drain directly to the Pacific, whereas rivers draining the eastern flank enter the sedimentary Cauca Basin at elevations of ~ 900–1,000 m, which serves as the baselevel for these rivers. Therefore, this contrast in χ is due to differences in baselevel and mostly disappears when a baselevel of 950 m is used for calculation (Fig. S5).

North of the slab tear, multiple knickpoints are located mostly at the margins of the low–relief surfaces in the northern Central Cordillera, where rivers leave the low–relief surfaces of the Antioqueño Plateau and form steep canyons (Fig. 5A). Knickpoint elevations within a region are similar but decrease in elevation towards the east (Fig. 5D, E), mimicking the swath profile in Fig. 2B. The position of knickpoints is not controlled lithology, nor faulting as the granites and gneisses that comprise the vast majority of the AP have similar erodibilities and knickpoints do not align with active faults (Fig. 5B). River profiles in the northern Western Cordillera are mostly well graded and rarely exhibit knickpoints, though rivers draining the northernmost part of the Western Cordillera seem to have a higher concavity compared to the rest of the Northern Andes (Fig. 5C).

There are fewer knickpoints south of the slab tear and the river profiles draining the flanks of the Central Cordillera are mostly well graded (Fig. 6 A, D). Knickpoints are often located around volcanic plateaus, e.g., of the Ruiz–Tolima Volcanic Massif, where Pliocene and Quaternary volcanic rocks infill valleys, and near transitions from volcanic fields to the underlying basement rocks (Fig. 6B). In the southern Central Cordillera, a low relief region with knickpoints following its margin is located along the crest of the Andes. This low–relief area is bounded in the west by the Silvia-Pijão Fault (Fig. 6B) and may therefore be related to fault activity. However, ubiquitous u-shaped valleys above the knickpoints suggest that glaciation could have contributed to the lower gradient. Herd (1975) and Thouret et al. (1997) found that glaciers during the last glacial maximum, terminated mostly between 3,000-3,200 m, with some glaciers advancing down to ~ 2,700 m on the eastern flank. We highlight the 3,200 m contour line in Fig. 6A and find that it mostly outlines the low-relief surfaces in the southern Central Cordillera. The Western Cordillera does not exhibit clear differences in its drainage network north and south of the slab tear. Drainages in the southern Western Cordillera are still mostly well graded with some knickpoints that may be attributed to lithology and some related to small-scale drainage reorganization (Fig. 6C).

4.3 Cauca and Patía river profiles and erosion rate data

The overall shape of the longitudinal profile of the main trunk of the Cauca River also shows differences across the slab tear (Fig. 7A,B). South of the slab tear, the Cauca River profile has a low-gradient concave up form as it flows through an intermontane sedimentary basin. Close to the location of the proposed slab tear, the Cauca River steepens and entrenched into a canyon, where it maintains high steepness throughout. The Patía River profile is similar to the Cauca, where the river flattens past its headwaters to a base level that is ~400 m lower than the Upper Cauca valley. As the Patía river starts flowing across the Western Cordillera, its profile steepens again, and the river forms a deep canyon. In the lower segment, higher channel steepness is likely related to the higher erosional resistance of the Western Cordillera basement rocks (Fig. 7B,C) and higher uplift rates past the orogen bounding thrust faults.

The differences in steepness, χ, and other topographic metrics along the main river profiles are reflected in the erosion rate estimates from suspended load data (Fig. 7D). In the Cauca River Basin, the erosion rate at the lower gauge station, draining both the upper segment of the Cauca Basin and the steep Cauca Canyon, is about six times higher than that of the Upper Cauca Valley (Fig. 7D). The area upstream of the lower gauge has a drainage area of $5.63 \times 10^4 km^2$ and a mean decadal erosion rate of ~1,207±560 m/My, while the upper pourpoint of the Cauca River Basin has a drainage area of $2.63 \times 10^4 km^2$ and a mean decadal erosion rate of ~208±107 m/My. The data from the upper Cauca River station provides an estimate of the erosion rate in the upper segment of the basin, located south of the slab tear, whereas the data from the station located on the lower segment of the Cauca River provides an estimate of the erosion rate in the entire Cauca basin. We can calculate the erosion rate only for the lower segment of the Cauca basin, the segment of the Central Cordillera north of the slab tear, as follows:

$$(5)\ \boldsymbol{\varepsilon_{lc}} = \left(\boldsymbol{\varepsilon_c} - \boldsymbol{\varepsilon_{uc}} * \frac{A_{uc}}{A_c}\right) * \left(\frac{A_c - A_{uc}}{A_c}\right)^{-1}$$

Where ε_c, ε_{uc}, and ε_{lc} are the decadal erosion rates from the entire Cauca basin, the upper basin, and the lower basin respectively and A represents the catchment area for each of these segments of the Cauca Basin. Using this equation, the erosion rate for the segment of the Central Cordillera north of the slab tear, the lower Cauca, is 2,200±570 m/Myr.

The Patía River erosion rate is higher than the upper segment of the Cauca River basin, thereby corroborating the divide migration predicted by topographic metrics (Figs. 3A and 4B). The pour point of the Upper Patía River has a drainage area of $1.23x10^4 km^2$ and a mean decadal erosion rate of ~560±326 m/My.

4.4 Evidence of Pliocene to modern basin infilling and incision in the Patía Basin

Field observations, as well as the geological map in Fig. 8, show that in several areas of the Patía Basin, high volumes of Pliocene to Holocene lavas, pyroclastic and volcaniclastic rocks, sourced from the volcanic edifices to the Central Cordillera were deposited. These deposits bury paleo-topography and fill paleo-valleys (Fig. 8C–E). The emplacement of large volumes of volcanic rocks near the modern drainage divide between the Cauca and Patía rivers may have blocked and diverted streams. The Patía and its tributaries have incised hundreds of meters into these volcanic deposits and thereby present an opportunity to estimate fluvial incision rates within the Patía Basin.

The headwaters of the Patía and Cauca rivers are in the Popayan Plateau (Fig. 8A). This plateau is formed by Pleistocene–Quaternary lavas, pyroclastic and volcano sedimentary rocks that have a local thickness >400 m. Thus, they contributed significantly to the formation of the topography at the drainage divide. The timing of formation of the Popayan Plateau is constrained by Ar-Ar geochronology on the volcanic rocks of the Popayan Formation to 1.6±0.8 to 2.9±0.3 Ma (Figure 8B,C; Table S2; Risnes, 1995; Torres Hernández, 2010).

The Patía River is the only river that crosses the Western Cordillera and has a strong bend ("elbow"), where it deviates from the N-S structurally controlled flow and crosses the Western Cordillera through a narrow canyon (i.e., "Hoz de Minamá" canyon; Fig. 8A). The location of this canyon coincides with a local depression in the Western Cordillera, where remnants of perched volcanic deposits of Pleistocene age unconformably overlie the oceanic basement of the Western Cordillera (Fig. 8E,G,H) at elevations of ~ 0.5 km above the modern channel. To the east, in the Juanambu Canyon (tributary of the Patía) a thick volcanic sequence has been deposited and now is being dissected by the Juanambu River (Fig. 8D). The top of the volcanic deposits in the Juanambu Canyon is located ~500 m above the modern river. The age of the volcanic deposits in the Hoz de Minamá and the Juanambu Canyon is unconstrained, but assuming a Pleistocene age (ca. 1.5±0.1 Ma) based on the correlation of these deposits with nearby ignimbrites (A. Murcia and Cepeda, 1991; Murcia and Pichler, 1986), allows us to estimate an incision rate of ~ 0.3 km/Myr for both rivers since the emplacement of the volcanic deposits.

The cross section in figure 8C shows the relationship between the volcanic deposits of the Popayan Plateau and the other volcanics along the Patía River. The base of the Plio-Quaternary volcanic rocks of the Popayan plateau aligns with the elevations of the lava flows and volcaniclastics perched along and at the outlet of the Upper Patía Valley. The flat pre-volcanic topography resembles the low gradient of the Upper Cauca Valley just north of the Popayan Plateau. The lack of pre-volcanic topography along the modern drainage divide between the Cauca and Patía Rivers suggests that their drainage basins may have been connected before the emplacement of up to 400m of volcanics. We hypothesize that the high rates of emplacement of volcanics around the Popayan Plateau could have disrupted a north-flowing paleo-Patía-Cauca River in the Pleistocene and caused overflow of the Patía river into the Pacific Ocean. This capture would have substantially lowered base level in the Patía basin and caused the incision we documented along the Hoz de Minamá and the Juanambu canyons; we further discuss this potential capture in section 5.2.

5. Discussion

Our geomorphic analysis shows spatial variations in topography and drainage network metrics along the Western and Central Cordilleras of the Northern Andes of Colombia. In the following sections we discuss the processes involved in driving these variations. We first discuss large-scale variations that may be linked to subduction geometry and subsequently examine local variations linked to volcanism. Finally, we discuss our findings in the context of regional biodiversity.

5.1 Topographic response to spatial and temporal changes in slab geometry

5.1.1 Landscape and river response

We have documented a series of knickpoints surrounding low-relief high-elevation areas in the Central Cordillera, north of the slab tear. Given the absence of active faulting, lithologic and climatic variations across knickpoints and considering their alignment in elevation (Fig. 5E), we interpret these knickpoints as indicators of a temporal change in uplift rate. South of the slab tear, rivers in the Central Cordillera are mostly well graded suggesting more constant rates of uplift through time. This is similar to the Western Cordillera, where χ-profiles document roughly constant channel steepness in agreement with constant uplift through time. The interpretation of an increase in uplift rate north of the slab tear is supported by the Cauca River profile. Close to the proposed location of the slab tear, the Cauca River steepness increases dramatically and transitions from the low gradient plains of the Upper Cauca valley to the up to 2.5 km deep Cauca Canyon (Fig. 7B,C). This topographic change coincides with a downstream increase in catchment wide erosion rates observed in gauge data along the Cauca River which supports the idea of differences in rock uplift rates north and south of the slab tear. The uplift signal seems to decay towards the east, away from the Romeral Fault zone as indicated by the tilt of the east-sloping low relief region in our swath profiles (Fig. 2A) and the accompanying gradual lowering of knickpoint elevations (Fig. 5E).

Despite the trend of well graded rivers in the Central Cordillera south of the slab tear, we document two exceptions to this general behavior. The Ruiz-Tolima Volcanic Massif (Cordillera Central) encompasses an area of lower relief with several knickpoints. Here, the Pliocene to modern volcanic rocks form landscapes with lower gradients and infill paleo-valleys. Knickpoints are commonly located around these volcanic complexes, suggesting that the emplacement of volcanic rocks may be responsible for the observed topography. Another low relief surface with knickpoints is located in the southern Central Cordillera, south of the volcanic complexes (Fig. 6A). Its western border seems to follow the Silvia-Pijao Fault, suggesting that increased fault slip may have contributed to the uplift of this low relief region. It is noteworthy, that especially along the eastern margin of this area, river valleys are u-shaped, suggesting that glaciation of this region may have lowered the gradients of upper river reaches (e.g., Brocklehurst and Whipple, 2007) and may, therefore, be another contributor to the formation of low relief regions with knickpoints. The modern equilibrium line altitude (ELA) in the Ruiz–Tolima volcanic massif is located at ca. 5,100 m (see Thouret et al., 1997 and references therein). However, the glaciers terminated at elevations as low as ca. 2,900–3,300 m during the last glacial maximum (Herd, 1975; Thouret et al., 1997). Based on the close correlation of this elevation band with the outline of the low-relief surfaces in the southern Cordillera Central, we propose that glaciers contributed to the observed lower gradient of high elevation topography.

5.1.2 Drainage reorganization

Our analysis shows that rivers draining the western flank of the northern Central Cordillera are capturing drainage area from east-flowing rivers perched on the Antiqueño Plateau. This is supported by differences in χ-values across the drainage divides and topographic steepness values, yet additional evidence can be found along the Porce River. In contrast to all its tributaries, that exhibit major knickpoints as they flow onto the Antiqueño Plateau, the Porce River flows through a >1 km deep canyon that cuts through the entire Antiqueño Plateau and suddenly ends without clearly defined headwaters (Fig. 9). The channel steepness of the upper Porce River is substantially lower than that of its tributaries or the neighboring Cauca Canyon. The occurrence of this deeply dissected valley without headwaters, in a region where divide migration towards the east is predicted, suggests that this is likely a drainage capture location, where the Porce was once part of the paleo-Cauca River. Now, the Porce River is a minor stream that flows through a >1 km deep canyon referred to as the Aburra Valley, the only canyon crossing the entire Antioqueño Plateau. This suggests that a river with far greater erosive power than the modern Porce River was responsible for carving this valley (Fig. 9). We therefore hypothesize that the Aburra Valley is where the paleo-Cauca River flowed before and during the initial increase in uplift rate. As the largest river of this region, the paleo-Cauca River would have had the erosional power to carve this canyon, after the onset of the increase in uplift rate. At some point, uplift along the Romeral Fault Zone (Fig. 1B) likely exceeded the erosional capacity of the paleo-Cauca or it was captured by headward erosion of a stream following the path of the modern Cauca Canyon. The uneroded steep canyon walls of the Aburra Canyon and the lack of tributary incision suggest that the formation of this canyon was comparatively recent and fast. If the hypothesis is correct, this capture would have shifted the locus of sedimentation at the outlet of the Cauca River by about 60 km to the west (Fig. 9). Furthermore, the elevation difference between the upstream end of the paleo-Cauca channel along the modern Porce and the downstream end of the modern Cauca Valley suggest > 800m of differential uplift of the region north of the slab tear since the capture (Fig. 9).

Previous thermochronology work in the walls of the Aburra Valley (Porce River Canyon) revealed older Paleogene AHe and AFT ages but was unable to reveal the age of incision of the canyons (Restrepo-Moreno et al., 2009a; Saenz, 2003; Villagómez and Spikings, 2013). We speculate that the absence of younger ages in the Porce River Canyon could be explained if its incision was recent (<10 Ma) but the magnitude of incision (~1 km) was insufficient to reach the younger cooling ages below the pre-incision Partial Retention (or Annealing) Zone (e.g., Fitzgerald and Malusà, 2019 and references therein).

5.1.3 Slab flattening as probable cause for uplift rate change and comparison with previous studies

From our topographic analysis we infer a recent increase in uplift rate in the northern Central Cordillera. Neogene tectonic events in this region that may have caused this change, include the collision Panamá-Chocó block (15–12 Ma; Farris et al., 2011; León et al., 2018;

Montes et al., 2015, 2012) and flattening of the subducting slab <9 Ma ago (Wagner et al., 2017). The differences we observed in river profiles and relief distribution along the Central Cordillera and Cauca Valley, show a close spatial correlation with the proposed location of the slab tear and the main area of slab flattening (Fig. 10). We did not find topographic differences along the Western Cordillera that correlate with proximity to the Panamá-Chocó block collision zone. Therefore, we propose that slab flattening in the northernmost part of the Nazca subduction zone caused an increase of rock and surface uplift in the northern Cordillera Central. The initiation of the slab tear that separates the flat and normal dipping sections of the Nazca Plate is located below the Western Cordillera (Wagner et al., 2017). We hypothesize that changes of slab geometry below the Western Cordillera were minor, resulting in the observed lack of clear along-strike differences in topography.

Flat slab subduction has been suggested to increase the coupling between tectonic plates and in response increase crustal shortening that may induce surface uplift (Eakin et al., 2014; Espurt et al., 2008). In contrast, Martinod et al. (2020) propose that flat slab subduction acts to promote deformation above the downdip end of the flat slab segment, with limited crustal thickening above the flat lying part. Numerical modelling and field observations in the Peruvian flat slab have documented that the transition from normal to flat slab subduction may result in a "dynamic uplift" from isostatic adjustments of >1.5 km in a ~250 km wide region directly above the flat slab (Eakin et al., 2014), without the need of crustal thickening. The elevation of the Antioqueño Plateau today is ~2.5 km and relief within the plateau is only a few hundred meters. The projection of the low gradient river profile sections on the Antioqueno Plateau suggest that the fluvial relief between the alluvial plain of the Magdalena River and the headwaters of the plateau rivers was on the order of 200 m (Fig. S6). Therefore, the total recent surface uplift can be assumed to be on the order of ~ 2 km, with a total width of the uplifting region of the Central Cordillera of ~160 km. This is in good agreement with the predictions from dynamic uplift (Eakin et al., 2014) with a potential contribution from increased crustal thickening.

We propose the following hypothesis for the tectonic evolution for the northern segment Central Cordillera during the Cenozoic. A period of high rock and surface uplift in the late Cretaceous–Paleogene associated with the collision of the Caribbean Plate with NW South America (León et al., 2021). In the early Miocene (ca. 18 Ma), the relief generated during the previous uplift phase would have been degraded to low elevations, forming the low-relief surfaces (e.g., Restrepo-Moreno et al., 2009b). In the late Miocene to Pliocene, the onset of flat slab subduction would have caused an increase in the rates of rock and surface uplift, elevating the low-relief surfaces to their modern elevation and driving subsequent river incision due to the induced base level fall. The fact that the rapidly uplifting northern part of the Central Cordillera lines up in strike with the supposedly older southern part of the Cordillera Central is likely related to the pre-existing structurally weak zones, e.g., the Romeral Fault zone already acted as a suture during the Paleogene accretion of Western Cordillera basement.

The hypothesis proposed here challenges the view that the Central Cordillera can be regarded as an old orogen with topography mostly established by the Paleogene (Bande et al., 2012; Gómez et al., 2003; Mora et al., 2019; Nie et al., 2012; Villagómez and Spikings, 2013). We speculate that topography in the southern Cordillera Central is indeed “old” (e.g., Villamizar-Escalante et al., 2021), whereas the topography in the northern Cordillera Central has only been growing since the Late Miocene to Pliocene. Yet, previous studies relying on thermochronology data were not able to identify this recent episode of mountain building, because uplift is too recent for the rivers in this region to have equilibrated their profiles and created sufficient incision.

Our landscape analysis in the Northern Andes shows that a major change in rock uplift rate in the northern Central Cordillera occurred as a result of the onset of flat-slab subduction north of 5°N. In fact, other geological information suggests a pulse of surface uplift of the northern segments of the Central and Western Cordilleras in the Neogene. For example, a recent study on the western flank of the Central Cordillera showed one thermal history model based on AFT thermochronology that shows an increase in exhumation at ~10 Ma (Duque-Palacio et al., 2021). A provenance analysis from the adjacent Middle Magdalena Valley to the east of the Central Cordillera, shows the appearance of a substantial proportion of detrital zircons with U-Pb ages <100 Ma in the upper Miocene Real Formation (Horton et al., 2015). These detrital zircons likely reflect contributions from Cretaceous to Paleogene igneous sources, typical of the rocks in the northern Central Cordillera and Western Cordillera (Horton et al., 2015). An AHe age of ~3.9 Ma in an Eocene batholith, that runs parallels to the Western Cordillera suggests active exhumation in the late Miocene-Pliocene (Villagómez and Spikings, 2013). Also, the detrital AFT age distribution of a sample from the western flank of the Western Cordillera has a significant Miocene age peak, with a handful of grains as young as 4.5 Ma (León et al., 2018).

Slab flattening also affected the deformation, exhumation, and topography of the Eastern Cordillera, which is in agreement with the prediction that slab flattening will induce deformation above the downdip hinge of the flat slab segment (Martinod et al., 2020). North of the slab tear the Eastern Cordillera reaches its maximum width, 250 km as opposed to 100 km south of the tear, and its highest elevations of up to 5 km in the Cocuy Range. Several thermochronology studies documented increased rates of exhumation since the Late Miocene to Pliocene (Mora et al., 2015, 2008; Parra et al., 2009; Siravo et al., 2019) in agreement with the general timing of slab flattening (Wagner et al., 2017). Increased surface uplift in the interior of the mountain range, similar to the northern Cordillera Central, is recorded by pollen studies in internally drained basins (Helmens and van der Hammen, 1994; Hooghiemstra et al., 2006), and by reworked pollen in the Llanos foreland basin (De La Parra et al., 2015). South of the slab tear, where the Eastern Cordillera is narrower, the structural style changes to uplifted basement blocks, which are tilted monoclines of reduced width (Saeid et al., 2017). Also, the faults in this region record less displacement compared to faults north of the slab tear (Mora et al., 2008, 2006; Pérez-Consuegra et al., 2021; Saeid et al., 2017).

However, an important observation is that the location of the trace of the suggested slab tear (Chiarabba et al., 2016; Wagner et al., 2017) does not coincide with the structural segmentation suggested by Mora et al. (2008). While the slab tear is located roughly at 5°N the plateau style of deformation extends southwards up to about 4°N. This could be reconciled if we consider that structural domains in the upper plate may not coincide exactly with the segmentation of the lower subducting plate. We hypothesize that the late Miocene plateau style of uplift within the Eastern Cordillera could be highly controlled by the areal extent and inherited structures of the former early Cretaceous rift (e.g., Mora et al., 2006; Pérez-Consuegra et al., 2021). The compression generated from below caused by the subducting plate could be located north of 5°N but the effects on uplift of the upper plate could reach more southerly regions even up to 4°N because that is the southern end of the early Cretaceous rift domain which would have behaved as a single tectonic province or coherent block (Carrillo et al., 2016; e.g., Mora et al., 2006; Pérez-Consuegra et al., 2021), which is probably analogous to the uplifted region of the northern Central Cordillera.

5.2 Drainage reorganization caused by volcanism

The onset of flat slab subduction ended arc volcanism in the northern Central and Western Cordillera, whereas volcanism continued in the southern Cordillera Central. In the area near the Cauca–Patía divide, volcanism plays an important role in ongoing drainage reorganization through the development of a Quaternary volcanic plateau that acts as a barrier, separating the upper Cauca from the upper Patía basins. Today, the differences in χ, channel steepness and hillslope gradient across the Cauca–Patía divide suggest that the Patía Basin is capturing drainage area from the headwaters of the Cauca River (Figs. 3,4). The presence of highly dissected Pliocene–Quaternary volcanic deposits in the Patía River catchment implies active fluvial incision. consistent with the high decadal erosion rate in the Patía Basin (506 m/Myr) derived from gauge data. Erosion rates in the adjacent Cauca basin are a factor of 2 lower (Fig. 7). The gauge derived erosion rate estimates may be higher than the true values due to the human influence on the landscapes such as land degradation and deforestation (Restrepo and Cantera, 2013), but without cosmogenic nuclide derived erosion rates, these serve as a first order estimate. Also, the Salvajina Reservoir, built in 1985, is located upstream of the upper Cauca station (Figure 7) and the sediment load observations used to build the rating curve for the upper Cauca station were made after 1998 (Table S1). Therefore, the estimated decadal erosion rates from this study could be underestimating the actual erosion rates values in the upper Cauca catchment due to sediment storage in the reservoir (e.g., Latrubesse et al., 2017).

We explain the apparent high erosion rate and low χ values of the Patía River, as part of a transient wave of erosion resulting from the capture of a segment of the southern extreme of the ancient Cauca River (Fig. 10). The pre-volcanic topography of the Upper Patía Valley and the area of the Patía-Cauca drainage divide have very low gradients. This is in contrast with the modern topography, where the Upper Patía Valley shows substantially higher relief and slopes compared to the Upper Cauca Valley. The change in topography in the region of the modern drainage divide since the late Pliocene to Pleistocene between the Upper Cauca and Upper Patía Valleys supports the idea of drainage capture. Faulting and differential vertical movement after the emplacement of volcanic rocks may have affected the reconstructed pre-volcanic topography (Fig. 8C, 10A,B), yet the geologic map does not show any faults with significant throw throughout the Quaternary along our profile line (Gómez et al., 2015). Moreover, the alignment in elevation of volcanic rocks perched above the outlet of the Upper Patía Valley and the thick Popayan Plateau volcanic sequence, suggests that capture of the Patía River from a paleo-Patía-Cauca River is feasible (Fig. 10).

Two mechanisms offer plausible explanations for the capture of the ancient Cauca's headwaters (e.g., Larson et al., 2017): (1) Basin overflow or spillover. In this scenario, the high rates of volcaniclastic infilling of the Patía drainage basin during the Pliocene to Quaternary would have caused a spill-over towards the Pacific basin, creating a connection between the Pacific and the former Upper Cauca Basin through a low point in the Western Cordillera; or (2) a river draining the western flank of the Western Cordillera eventually captured the former Cauca-Patía drainage basin through headward erosion.

Initially, the Patía-Cauca River would have flowed N-S following geological structures as the Cauca River today does over most of its course without a connection to the Pacific Ocean. Drainage capture to the Pacific would have lowered the base level of the Patía significantly. This is supported by the deep incision of volcanic rocks perched above the canyons of the Patía and its tributaries (Fig. 8D, E) and contrasts the Cauca intermontane basin that is actively alluviating. Evidence for a former fluvial connection between the Cauca and Patía Rivers was suggested previously based on the geomorphic evidence (e.g., Padilla and Leon, 1989) and the similarity amongst the fish faunas in both basins (Maldonado-Ocampo et al., 2012, e.g., 2005). According to Maldonado-Ocampo et al. (2005) eleven species of fish are shared between the upper Cauca and Patía Basins. A modern analogue for a low point in the Western Cordillera that could lead to drainage capture can be found near the city of Cali (Fig. S7), where the distance between the drainage divide and the Cauca River is <5 km.

5.3 Implications of recent topographic growth and drainage reorganization on the biodiversity of the Northern Andes

We have provided evidence for changes in topography and drainage reorganization associated with the onset of flat-slab subduction and volcanism that may have impacted biodiversity in the Northern Andes. The implications of our findings can be tested using species distribution or phylogenetic data (e.g., Baker et al., 2014). Prior to the onset of the flat-slab subduction, the northern Central Cordillera was a low-lying tropical environment. This is supported by the projection of above knickpoint river profiles from the Antioqueño Plateau (Fig. S6), slow exhumation rates from thermochronology (Restrepo-Moreno et al., 2009a; Villagómez and Spikings, 2013), and palynology from the Pliocene Mesas Formation (Dueñas and Castro, 1981). Since the onset of flat subduction at ca. 4–8 Ma this region went from tropical lowlands to ~2.5 km elevation at a minimum rate of 250 m/Myr. The uplift of the northern Central Cordillera may have isolated former lowland species at high elevations and led to an increased heterogeneity of the landscape by generating a wide variety of climates and ecosystems.

In fact, the Antioqueño Plateau is a place of high alpha biodiversity (Graham et al., 2018) and a distinct biogeographic region within the Central Cordillera (Hazzi et al., 2018). Furthermore, pool-water species fish documented on the Antioqueño Plateau lack the ability to disperse from the tropical lowlands along steep mountain rivers (Jaramillo-Villa et al., 2010), along with a generally high degree of fish endemism (Tognelli et al., 2016). This high diversity was enigmatic for ecologists in the past because the older thermochronology ages of the northern Central Cordillera were interpreted as low exhumation rates and little topographic change in the past ca. 25 Ma (Graham et al., 2018). Therefore, other factors such as nutrient rich soils (Hermelin, 2015) derived from igneous rocks and a quaternary volcanic horizon in the Central Cordillera were suggested as factors that could contribute to the high regional diversity (Graham et al., 2018). The topographic changes and drainage reorganization in the northern segment of the Central Cordillera predicted by our data for the past 10 Ma could explain these biodiversity patterns. Events of drainage capture and reorganization can create new habitat connections and barriers for aquatic species and lead to speciation (e.g., Stokes and Perron, 2020). This could explain the shared distribution of species in between the upper segments of the Cauca and Patía rivers (Maldonado-Ocampo et al., 2012, 2005).

6. Conclusions

In this paper we used geomorphic observations to understand how the topography of the Central and Western cordilleras of the Northern Andes were affected by recent changes in slab geometry and drainage reorganization. We find the following conclusions:

1. The northern segment of the Central Cordillera is characterized by an elevated low-relief surface with roughly uniform lithology and surrounded by multiple knickpoints. The transition to this topography coincides with an increase in channel steepness and decadal erosion rates along the Cauca River. These geomorphic features suggest a recent increase in rock and surface uplift rate in the northern Central Cordillera.

2. Slab flattening north of 5°N is the most likely cause of the recent ~2 km of surface uplift since 8–4 Ma in the northern Central Cordillera.

3. Large scale drainage reorganization of major rivers has occurred in the Northern Andes in the past 10 Ma. In the northern segment of the ranges the drainage reorganization is driven by changes in upper plate deformation in relation to development of the flat slab subduction geometry. However, to the south of the range other factors such as emplacement of volcanic rocks likely play important roles in this process.

4. The evidence of Miocene to present changes in the elevation of the northern Central Cordillera and the drainage reorganization in the Cauca and Patía basins presented in this study may have left an imprint in the modern distribution of species. These findings offer geologic scenarios that together with biological data could be used to elucidate the imprint of regional landscape evolution on freshwater fish diversification and of high alpha diversity regionally.

Acknowledgements

Thanks to C. Do Nascimento, C. Montes, D. Scherler, S. Echeverri for discussions regarding geological and biological aspects of the study area. We thank the late J. Maldonado for his work with Andean freshwater fish that inspired us. M. Rodríguez, A. Fernandez, A. Cuervo and A. Rodríguez-Corcho for help making observations during the field work. Thanks to S.J. Rios for help with figures.

N.P. was funded by a 2018 National Geographic Early Career Grant (EC-51182R-18), a 2018 Grants in Aid award from the American Association of Petroleum Geologists, a 2019 Graduate Student Grant from the Geological Society of America, the 2020 Student Grant from the Central New York Association of Professional Geologists, the Geo.X Travel Grant (Germany), the K. D. Nelson Nelson Summer Research Fund from the Department of Earth Sciences, a Syracuse University Graduate Student Fellowship, a "Research Excellence Doctoral Fellowship" Graduate Student Fellowship at Syracuse University, and a grant from the "Fundación para la Promoción de la Investigación y la Tecnología (FPIT)" Banco de la República (Colombia). The work of J.P.G. and J.V.P. was founded by the Spanish Ministry of Science and Innovation (MICINN) through the projects "PID2019-107138RB-I00 / AEI / 10.13039/501100011033" and "RYC-2017-23335". R.O. is funded by a Swiss National Science Foundation fellowship, grant number P2EZP2_191866. We thank L. Husson and an anonymous reviewer for comments that helped to improve this manuscript.

References

Alfonso, C.A., Sacks, P.E., Secor, D.T., Rine, J., Perez, V., 1994. A tertiary fold and thrust belt in the Valle del Cauca Basin, Colombian Andes. J. South Am. Earth Sci. 7, 387–402. doi:10.1016/0895-9811(94)90023-X

Antonelli, A., Kissling, W.D., Flantua, S.G.A., Bermúdez, M.A., Mulch, A., Muellner-Riehl, A.N., Kreft, H., Linder, H.P., Badgley, C., Fjeldså, J., Fritz, S.A., Rahbek, C., Herman, F., Hooghiemstra, H., Hoorn, C., 2018. Geological and climatic influences on mountain biodiversity. Nat. Geosci. 11, 718–725. doi:10.1038/s41561-018-0236-z

Antonelli, A., Sanmartín, I., 2011. Why are there so many plant species in the Neotropics? Taxon 60, 403–414. doi:10.2307/41317138

Aspden, J.A., McCourt, W.J., 1986. Mesozoic oceanic terrane in the central Andes of Colombia. Geology 14, 415–418. doi:10.1130/0091-7613(1986)14<415:motitc>2.0.co;2

Aspden, J.A., McCourt, W.J., Brook, M., 1987. Geometrical control of subduction-related magmatism: the Mesozoic and Cenozoic plutonic history of Western Colombia. J. Geol. Soc. London. 144, 893–905. doi:10.1144/gsjgs.144.6.0893

Badgley, C., Smiley, T.M., Terry, R., Davis, E.B., DeSantis, L.R.G., Fox, D.L., Hopkins, S.S.B., Jezkova, T., Matocq, M.D., Matzke, N., McGuire, J.L., Mulch, A., Riddle, B.R., Roth, V.L., Samuels, J.X., Strömberg, C.A.E., Yanites, B.J., 2017. Biodiversity and Topographic Complexity: Modern and Geohistorical Perspectives. Trends Ecol. Evol. 32, 211–226. doi:10.1016/j.tree.2016.12.010

Baker, P.A., Fritz, S.C., Dick, C.W., Eckert, A.J., Horton, B.K., Manzoni, S., Ribas, C.C., Garzione, C.N., Battisti, D.S., 2014. The emerging field of geogenomics: Constraining geological problems with genetic data. Earth-Science Rev. 135, 38–47. doi:10.1016/j.earscirev.2014.04.001

Bande, A., Horton, B.K., Ramírez, J.C., Mora, A., Parra, M., Stockli, D.F., 2012. Clastic deposition, provenance, and sequence of Andean thrusting in the frontal Eastern Cordillera and Llanos foreland basin of Colombia. Bull. Geol. Soc. Am. 124, 59–76. doi:10.1130/B30412.1

Brocklehurst, S.H., Whipple, K.X., 2007. Response of glacial landscapes to spatial variations in rock uplift rate. J. Geophys. Res. 112, F02035. doi:10.1029/2006JF000667

Carretier, S., Tolorza, V., Regard, V., Aguilar, G., Bermúdez, M.A., Martinod, J., Guyot, J.L., Hérail, G., Riquelme, R., 2018. Review of erosion dynamics along the major N-S climatic gradient in Chile and perspectives. Geomorphology 300, 45–68. doi:10.1016/j.geomorph.2017.10.016

Carrillo, E., Mora, A., Ketcham, R.A., Amorocho, R., Parra, M., Costantino, D., Robles, W., Avellaneda, W., Carvajal, J.S., Corcione, M.F., Bello, W., Figueroa, J.D., Gómez, J.F., González, J.L., Quandt, D., Reyes, M., Rangel, A.M., Román, I., Pelayo, Y., Porras, J., 2016. Movement vectors and deformation mechanisms in kinematic restorations: A case study from the Colombian Eastern Cordillera. Interpretation 4, T31–T48. doi:10.1190/INT-2015-0049.1

Cediel, F., Shaw, R.P., Cáceres, C., 2005. Tectonic assembly of the Northern Andean Block. AAPG Mem.

Chiarabba, C., De Gori, P., Faccenna, C., Speranza, F., Seccia, D., Dionicio, V., Prieto, G.A., 2016. Subduction system and flat slab beneath the Eastern Cordillera of Colombia. Geochemistry, Geophys. Geosystems 17, 16–27. doi:10.1002/2015GC006048

Dávila, F.M., Lithgow-Bertelloni, C., 2013. Dynamic topography in South America. J. South Am. Earth Sci. 43, 127–144. doi:10.1016/j.jsames.2012.12.002

De La Parra, F., Mora, A., Rueda, M., Quintero, I., 2015. Temporal and spatial distribution of tectonic events as deduced from reworked palynomorphs in the eastern Northern Andes. Am. Assoc. Pet. Geol. Bull. 99, 1455–1472. doi:10.1306/02241511153

Dueñas, H., Castro, G., 1981. Asociación palinológica de la Formación Mesa en la región de Falán, Tolima, Colombia. Geol. Norandina 3, 27–36.

Duque-Caro, H., 1990. Neogene stratigraphy, paleoceanography and paleobiogeography in northwest South America and the evolution of the Panama seaway. Palaeogeogr. Palaeoclimatol. Palaeoecol. 77, 203–234. doi:10.1016/0031-0182(90)90178-A

Duque-Palacio, S., Seward, D., Restrepo-Moreno, S.A., García-Ramos, D., 2021. Timing and rates of morpho-tectonic events in a segment of the Central and Western cordilleras of Colombia revealed through low-temperature thermochronology. J. South Am. Earth Sci. 106, 103085. doi:10.1016/j.jsames.2020.103085

Eakin, C.M., Lithgow-Bertelloni, C., Dávila, F.M., 2014. Influence of Peruvian flat-subduction dynamics on the evolution of western Amazonia. Earth Planet. Sci. Lett. 404, 250–260. doi:10.1016/j.epsl.2014.07.027

Echeverri, S., Cardona, A., Pardo, A., Monsalve, G., Valencia, V.A., Borrero, C., Rosero, S., López, S., 2015. Regional provenance from southwestern Colombia fore-arc and intra-arc basins: Implications for Middle to Late Miocene orogeny in the Northern Andes. Terra Nov. 27, 356–363. doi:10.1111/ter.12167

Ego, F., Sébrier, M., Yepes, H., 1995. Is the Cauca-Patia and Romeral Fault System left or rightlateral? Geophys. Res. Lett. 22, 33–36. doi:10.1029/94GL02837

Espurt, N., Funiciello, F., Martinod, J., Guillaume, B., Regard, V., Faccenna, C., Brusset, S., 2008. Flat subduction dynamics and deformation of the South American plate: Insights from analog modeling. Tectonics 27, 1–19. doi:10.1029/2007TC002175

Farris, D.W., Jaramillo, C., Bayona, G., Restrepo-Moreno, S.A., Montes, C., Cardona, A., Mora, A., Speakman, R.J., Glascock, M.D., Valencia, V., 2011. Fracturing of the Panamanian Isthmus during initial collision with South America. Geology 39, 1007–1010. doi:10.1130/G32237.1

Fitzgerald, P.G., Malusà, M.G., 2019. Concept of the Exhumed Partial Annealing (Retention) Zone and Age-Elevation Profiles in Thermochronology, in: Malusà, M.G., Fitzgerald, P.G. (Eds.), Springer Textbooks in Earth Sciences, Geography and Environment. Springer International Publishing, Cham, pp. 165–189. doi:10.1007/978-3-319-89421-8_9

Forte, A.M., Whipple, K.X., 2018. Criteria and tools for determining drainage divide stability. Earth Planet. Sci. Lett. 493, 102–117. doi:10.1016/j.epsl.2018.04.026

Gallego–Ríos, A.F., Pardo–Trujillo, A., López–Plazas, G.A., Echeverri, S., 2020. The Morales Formation (new unit): Record of fluvial–lacustrine environments and the beginning of the Miocene explosive volcanism in the Patía Sub–basin (SW Colombia), in: Gómez, J., Mateus–

Zabala, D. (Eds.), The Geology of Colombia, Volume 3 Paleogene – Neogene. Bogotá, pp. 395–415. doi:10.32685/pub.esp.37.2019.13

Garzione, C.N., McQuarrie, N., Perez, N.D., Ehlers, T.A., Beck, S.L., Kar, N., Eichelberger, N., Chapman, A.D., Ward, K.M., Ducea, M.N., Lease, R.O., Poulsen, C.J., Wagner, L.S., Saylor, J.E., Zandt, G., Horton, B.K., 2017. Tectonic Evolution of the Central Andean Plateau and Implications for the Growth of Plateaus. Annu. Rev. Earth Planet. Sci. 45, 529–559. doi:10.1146/annurev-earth-063016-020612

Gómez, E., Jordan, T.E., Allmendinger, R.W., Hegarty, K., Kelley, S., 2005. Syntectonic Cenozoic sedimentation in the northern middle Magdalena Valley Basin of Colombia and implications for exhumation of the Northern Andes. Bull. Geol. Soc. Am. 117, 547–569. doi:10.1130/B25454.1

Gómez, E., Jordan, T.E., Allmendinger, R.W., Hegarty, K., Kelley, S., Heizler, M., 2003. Controls on architecture of the Late Cretaceous to Cenozoic southern. GSA Bull. 115, 131–147. doi:10.1130/0016-7606(2003)115<0131

Gómez, J., Nivia, Á., Montes, N.E., Diederix, H., Almanza, M.F., Alcárcel, F.A., Madrid, C.A., 2015. Mapa Geológico de Colombia, in: Gómez, J., Almanza, M.F. (Eds.), Compilando La Geología de Colombia: Una Visión a 2015. Servicio Geológico Colombiano. Publicaciones Geológicas Especiales No. 33. Bogotá, pp. 35–60.

Graham, C.H., Parra, M., Mora, A., Higuera, C., 2018. The Interplay between Geological History and Ecology in Mountains, in: Hoorn, C., Perrigo, A., Antonelli, A. (Eds.), Mountains, Climate and Biodiversity. John Wiley & Sons Ltd., pp. 231–243.

Gutscher, M.A., Spakman, W., Bijwaard, H., Engdahl, E.R., 2000. Geodynamics of flat subduction: Seismicity and tomographic constraints from the Andean margin. Tectonics 19, 814–833. doi:10.1029/1999TC001152

Hack, J.T., 1960. Interpretation of erosional topography in humid temperate regions. Am. J. Sci. 258, 80–97.

Hazzi, N.A., Moreno, J.S., Ortiz-Movliav, C., Palacio, R.D., 2018. Biogeographic regions and events of isolation and diversification of the endemic biota of the tropical Andes. Proc. Natl. Acad. Sci. 115, 7985–7990. doi:10.1073/pnas.1803908115

Helmens, K.F., van der Hammen, T., 1994. The Pliocene and Quaternary of the high plain of Bogotá (Colombia): A history of tectonic uplift, basin development and climatic change. Quat. Int. 21, 41–61. doi:10.1016/1040-6182(94)90020-5

Herd, D.G.D., 1975. Glacial and volcanic geology of the Ruiz-Tolima volcanic complex Cordillera Central, Colombia. Publicaciones Espec. del Ingeominas 1–48.

Hermelin, M., 2015. Landscapes and landforms of Colombia, Landscapes and Landforms of Colombia. doi:10.1007/978-3-319-11800-0

Hooghiemstra, H., Wijninga, V.M., Cleef, A.M., 2006. The Paleobotanical Record of Colombia: Implications for Biogeography and Biodiversity 1. Ann. Missouri Bot. Gard. 93, 297–325.

Hoorn, C., Wesselingh, F.P., ter Steege, H., Bermudez, M.A., Mora, A., Sevink, J., Sanmartin, I., Sanchez-Meseguer, A., Anderson, C.L., Figueiredo, J.P., Jaramillo, C., Riff, D., Negri, F.R., Hooghiemstra, H., Lundberg, J., Stadler, T., Sarkinen, T., Antonelli, A., 2010. Amazonia

Through Time: Andean Uplift, Climate Change, Landscape Evolution, and Biodiversity. Science 330, 927–931. doi:10.1126/science.1194585

Horton, B.K., 2018. Tectonic Regimes of the Central and Southern Andes: Responses to Variations in Plate Coupling During Subduction. Tectonics 37, 402–429. doi:10.1002/2017TC004624

Horton, B.K., Anderson, V.J., Caballero, V., Saylor, J.E., Nie, J., Parra, M., Mora, A., 2015. Application of detrital zircon U-Pb geochronology to surface and subsurface correlations of provenance, paleodrainage, and tectonics of the Middle Magdalena Valley Basin of Colombia. Geosphere 11, 1790–1811. doi:10.1130/GES01251.1

Howard, A.D., 1994. A detachment-limited model of drainage basin evolution. Water Resour. Res. 30, 2261–2285. doi:10.1029/94WR00757

Jaramillo-Villa, U., Maldonado-Ocampo, J.A., Escobar, F., 2010. Altitudinal variation in fish assemblage diversity in streams of the central Andes of Colombia. J. Fish Biol. 76, 2401–2417. doi:10.1111/j.1095-8649.2010.02629.x

Karger, D.N., Conrad, O., Böhner, J., Kawohl, T., Kreft, H., Soria-Auza, R.W., Zimmermann, N.E., Linder, H.P., Kessler, M., 2017. Climatologies at high resolution for the earth’s land surface areas. Sci. Data 4, 170122. doi:10.1038/sdata.2017.122

Kerr, A.C., Marriner, G.F., Tarney, J., Nivia, A., Saunders, A.D., Thirlwall, M.F., Sinton, C.W., 1997. Cretaceous Basaltic Terranes in Western Columbia: Elemental, Chronological and Sr-Nd Isotopic Constraints on Petrogenesis. J. Petrol. 38, 677–702. doi:10.1093/petroj/38.6.677

Kerr, A.C., Tarney, J., 2005. Tectonic evolution of the Caribbean and northwestern South America: The case for accretion of two Late Cretaceous oceanic plateaus. Geology 33, 269–272. doi:10.1130/G21109.1

Kerr, A.C., Tarney, J., Nivia, A., Marriner, G.F., Saunders, A.D., 1998. The internal structure of oceanic plateaus: inferences from obducted Cretaceous terranes in western Colombia and the Caribbean. Tectonophysics 292, 173–188. doi:10.1016/S0040-1951(98)00067-5

Larson, P.H., Meek, N., Douglass, J., Dorn, R.I., Seong, Y.B., 2017. How Rivers Get Across Mountains: Transverse Drainages. Ann. Am. Assoc. Geogr. 107, 274–283. doi:10.1080/24694452.2016.1203283

Latrubesse, E.M., Arima, E.Y., Dunne, T., Park, E., Baker, V.R., D'Horta, F.M., Wight, C., Wittmann, F., Zuanon, J., Baker, P.A., Ribas, C.C., Norgaard, R.B., Filizola, N., Ansar, A., Flyvbjerg, B., Stevaux, J.C., 2017. Damming the rivers of the Amazon basin. Nature. doi:10.1038/nature22333

León, S., Cardona, A., Parra, M., Sobel, E.R., Jaramillo, J.S., Glodny, J., Valencia, V.A., Chew, D., Montes, C., Posada, G., Monsalve, G., Pardo-Trujillo, A., 2018. Transition From Collisional to Subduction-Related Regimes: An Example From Neogene Panama-Nazca-South America Interactions. Tectonics 37, 119–139. doi:10.1002/2017TC004785

León, S., Monsalve, G., Bustamante, C., 2021. How Much Did the Colombian Andes Rise by the Collision of the Caribbean Oceanic Plateau? Geophys. Res. Lett. 48, 1–11. doi:10.1029/2021gl093362

Luebert, F., Weigend, M., 2014. Phylogenetic insights into Andean plant diversification. Front. Ecol. Evol. 2, 1–17. doi:10.3389/fevo.2014.00027

Maldonado-Ocampo, J.A., Ortega-lara, A., Usma Oviedo, J.S., Galvis Vergara, G., Villa-Navarro, F.A., Vazquez Gamboa, L., Prada-Pedreros, S., Rodríguez, C.A., 2005. Peces de los Andes de Colombia. Guía de campo. Instituto de Investigación de Recursos Biológicos Alexander von Humboldt, Bogotá D. C., Colombia.

Maldonado-Ocampo, J.A., Usma, J.S., Villa-Navarro, F.A., Ortega-Lara, A., Prada-Pedreros, S., Jiménez, L.F., Jaramillo-Villa, U., Arango, A., Rivas, T.S., Sánchez, G.C., 2012. Peces dulceacuícolas del Chocó biogeográfico. WWF Colombia, Bogotá DC, Colombia.

Malusà, M.G., Fitzgerald, P.G., 2019. From Cooling to Exhumation: Setting the Reference Frame for the Interpretation of Thermochronologic Data, in: Malusà, M., Fitzgerald, P. (Eds.), Fission-Track Thermochronology and Its Application to Geology. Springer, Cham, pp. 147–164. doi:10.1007/978-3-319-89421-8_8

Martinod, J., Gérault, M., Husson, L., Regard, V., 2020. Widening of the Andes: An interplay between subduction dynamics and crustal wedge tectonics. Earth-Science Rev. 204. doi:10.1016/j.earscirev.2020.103170

Montes, C., Bayona, G., Cardona, A., Buchs, D.M., Silva, C.A., Morón, S., Hoyos, N., Ramírez, D.A., Jaramillo, C.A., Valencia, V., 2012. Arc-continent collision and orocline formation: Closing of the Central American seaway. J. Geophys. Res. Solid Earth 117. doi:10.1029/2011JB008959

Montes, C., Cardona, A., Jaramillo, C., Pardo, A., Silva, J.C., Valencia, V., Ayala, C., Perez-Angel, L.C., Rodriguez-Parra, L.A., Ramirez, V., Nino, H., 2015. Middle Miocene closure of the Central American Seaway. Science 348, 226–229. doi:10.1126/science.aaa2815

Mora, A., Parra, M., Forero, G.R., Blanco, V., Moreno, N., Caballero, V., Stockli, D., Duddu, I., Ghorbal, B., Rodriguez Forero, G., Blanco, V., Moreno, N., Caballero, V., Stockli, D., Duddy, I., Ghorbal, B., Andres Mora, M.P.G.R.F.V.B.N.M.V.C.D.S.I.D.B.G., 2015. What drives orogenic asymmetry in the northern Andes?: A case study from the apex of the northern Andean orocline. AAPG Mem. 108, 547–586. doi:10.1306/13531949M1083652

Mora, A., Parra, M., Strecker, M.R., Kammer, A., Dimaté, C., Rodríguez, F., 2006. Cenozoic contractional reactivation of Mesozoic extensional structures in the Eastern Cordillera of Colombia. Tectonics 25, n/a-n/a. doi:10.1029/2005TC001854

Mora, A., Parra, M., Strecker, M.R., Sobel, E.R., Hooghiemstra, H., Torres, V., Jaramillo, J.V., 2008. Climatic forcing of asymmetric orogenic evolution in the Eastern Cordillera of Colombia. Bull. Geol. Soc. Am. 120, 930–949. doi:10.1130/B26186.1

Mora, A., Villagómez, D., Parra, M., Caballero, V.M., Spikings, R., Horton, B.K., Mora–Bohórquez, J.A., Ketcham, R.A., Arias–Martínez, J.P., 2019. Late Cretaceous to Cenozoic uplift of the northern Andes: Paleogeographic implications. Geol. Colomb. Vol. 3 Paleogene – Neogene 129–163. doi:10.32685/pub.esp.37.2019.04

Murcia, A, Cepeda, H., 1991. Geología de la plancha 410 La Unión. Departamento de Nariño. Escala 1:100.000.

Murcia, A., Cepeda, H., 1991. Plancha 410 La Unión, Mapa Geológico de Colombia. Ingeominas.

Murcia, A., Pichler, H., 1986. Geoquímica y dataciones radiométricas de las ignimbritas cenozoicas del SW de Colombia. Rev. CIAF.

Neuwerth, R., Suter, F., Guzman, C.A., Gorin, G.E., 2006. Soft-sediment deformation in a tectonically active area: The Plio-Pleistocene Zarzal Formation in the Cauca Valley (Western Colombia). Sediment. Geol. 186, 67–88. doi:10.1016/j.sedgeo.2005.10.009

Nie, J., Horton, B.K., Saylor, J.E., Mora, A., Mange, M., Garzione, C.N., Basu, A., Moreno, C.J., Caballero, V., Parra, M., 2012. Integrated provenance analysis of a convergent retroarc foreland system: U-Pb ages, heavy minerals, Nd isotopes, and sandstone compositions of the Middle Magdalena Valley basin, northern Andes, Colombia. Earth-Science Rev. 110, 111–126. doi:10.1016/j.earscirev.2011.11.002

Padilla, L., Leon, L., 1989. Aspector geológicos y geomorfológicos de como el rio Cauca corria hacia el sur. Boletín Geol. Colomb.

Paris, G., Machette, M.N., Dart, R.L., Haller, K.M., 2000. Map and database of Quaternary faults and folds in Colombia and its offshore regions. USGS Sci. Investig. Rep. 61.

Parra, M., Mora, A., Sobel, E.R., Strecker, M.R., González, R., 2009. Episodic orogenic front migration in the northern Andes: Constraints from low-temperature thermochronology in the Eastern Cordillera, Colombia. Tectonics 28, n/a-n/a. doi:10.1029/2008TC002423

Pennington, W.D., 1981. Subduction of the Eastern Panama Basin and seismotectonics of northwestern South America. J. Geophys. Res. Solid Earth 86, 10753–10770. doi:10.1029/JB086iB11p10753

Pérez-Consuegra, N., Hoke, G.D., Mora, A., Fitzgerald, P., Sobel, E.R., Sandoval, J.R., Glodny, J., Valencia, V., Parra, M., Zapata, S., 2021. The Case for Tectonic Control on Erosional Exhumation on the Tropical Northern Andes Based on Thermochronology Data. Tectonics 40. doi:10.1029/2020TC006652

Perron, J.T., Royden, L., 2013. An integral approach to bedrock river profile analysis. Earth Surf. Process. Landforms 38, 570–576. doi:10.1002/esp.3302

Rahbek, C., Borregaard, M.K., Colwell, R.K., Dalsgaard, B., Holt, B.G., Morueta-Holme, N., Nogues-Bravo, D., Whittaker, R.J., Fjeldså, J., 2019. Humboldt's enigma: What causes global patterns of mountain biodiversity? Science 365, 1108–1113. doi:10.1126/science.aax0149

Reiners, P.W., Brandon, M.T., 2006. Using Thermochronology To Understand Orogenic Erosion. Annu. Rev. Earth Planet. Sci. 34, 419–466. doi:10.1146/annurev.earth.34.031405.125202

Restrepo-Moreno, S.A., Foster, D.A., Stockli, D.F., Parra-Sánchez, L.N., 2009a. Long-term erosion and exhumation of the "Altiplano Antioqueño", Northern Andes (Colombia) from apatite (U-Th)/He thermochronology. Earth Planet. Sci. Lett. 278, 1–12. doi:10.1016/j.epsl.2008.09.037

Restrepo-Moreno, S.A., Foster, D.A., Stockli, D.F., Parra-Sánchez, L.N., 2009b. Long-term erosion and exhumation of the "Altiplano Antioqueño", Northern Andes (Colombia) from apatite (U-Th)/He thermochronology. Earth Planet. Sci. Lett. 278, 1–12. doi:10.1016/j.epsl.2008.09.037

Restrepo, J.D., Cantera, J.R., 2013. Discharge diversion in the Patía River delta, the Colombian Pacific: Geomorphic and ecological consequences for mangrove ecosystems. J. South Am. Earth Sci. 46, 183–198. doi:10.1016/j.jsames.2011.04.006

Restrepo, J.D., Kjerfve, B., 2002. Water Discharge and Sediment Load from the Western Slopes of the Colombian Andes with Focus on Rio San Juan. J. Geol. 108, 17–33. doi:10.1086/314390

Risnes, K., 1995. Géodynamique du sud-ouest des Andes colombiennes (dépression du Cauca-Patia) durant le Néogène : approche paléomagnétique. Université de Genève. Thèse. doi:10.13097/archive-ouverte/unige:98073

Royden, L., Perron, J.T., 2013. Solutions of the stream power equation and application to the evolution of river longitudinal profiles. J. Geophys. Res. Earth Surf. 118, 497–518. doi:10.1002/jgrf.20031

Saeid, E., Bakioglu, K.B., Kellogg, J., Leier, A., Martinez, J.A., Guerrero, E., 2017. Garzón Massif basement tectonics: Structural control on evolution of petroleum systems in upper Magdalena and Putumayo basins, Colombia. Mar. Pet. Geol. 88, 381–401. doi:10.1016/j.marpetgeo.2017.08.035

Saenz, E.A., 2003. Fission track thermochronology and denudational response to tectonics in the north of the Colombian Central Cordillera [Master’s thesis]. Shimane University Japan.

Scherler, D., Schwanghart, W., 2020. Drainage divide networks – Part 2: Response to perturbations. Earth Surf. Dyn. 8, 261–274. doi:10.5194/esurf-8-261-2020

Schildgen, T.F., Hoke, G.D., 2018. The Topographic Evolution of the Central Andes. Elements 14, 231–236. doi:10.2138/gselements.14.4.231

Schwanghart, W., Scherler, D., 2014. Short Communication: TopoToolbox 2-MATLAB-based software for topographic analysis and modeling in Earth surface sciences. Earth Surf. Dynam 2, 1–7. doi:10.5194/esurf-2-1-2014

Siravo, G., Faccenna, C., Gérault, M., Becker, T.W., Fellin, M.G., Herman, F., Molin, P., 2019. Slab flattening and the rise of the Eastern Cordillera, Colombia. Earth Planet. Sci. Lett. 512, 100–110. doi:10.1016/j.epsl.2019.02.002

Stokes, M.F., Perron, J.T., 2020. Modeling the evolution of aquatic organisms in dynamic river basins. J. Geophys. Res. Earth Surf. 0–2. doi:10.1029/2020jf005652

Suter, F., Sartori, M., Neuwerth, R., Gorin, G., 2008. Structural imprints at the front of the Chocó-Panamá indenter: Field data from the North Cauca Valley Basin, Central Colombia. Tectonophysics 460, 134–157. doi:10.1016/j.tecto.2008.07.015

Thouret, J.C., Van Der Hammen, T., Salomons, B., Juvigné, E., 1997. Late quaternary glacial stades in the Cordillera Central, Colombia, based on glacial geomorphology, tephra-soil stratigraphy, palynology, and radiocarbon dating. J. Quat. Sci. 12, 347–369. doi:10.1002/(sici)1099-1417(199709/10)12:5<347::aid-jqs319>3.0.co;2-%23

Tognelli, M.F., Lasso, C.A., Bota-sierra, C.A., Jiménez-segura, L.F., Cox, N.A. (Eds.), 2016. Estado de Conservación y Distribución de la Biodiversidad de Agua Dulce en los Andes Tropicales. Gland, Suiza, Cambridge, UK y Arlington, USA: UICN.

Torres Hernández, M.P., 2010. Petrografía, geocronología y geoquímica de las ignimbritas de la Formación Popoyán, en el context del vulcanismo del suroccidente de Colombia [Master's thesis]. Universidad EAFIT.

Trenkamp, R., Kellogg, J.N., Freymueller, J.T., Mora, H.P., 2002. Wide plate margin deformation, southern Central America and northwestern South America, CASA GPS observations. J. South Am. Earth Sci. 15, 157–171. doi:10.1016/S0895-9811(02)00018-4

Vargas, C.A., Mann, P., 2013. Tearing and Breaking Off of Subducted Slabs as the Result of Collision of the Panama Arc-Indenter with Northwestern South America. Bull. Seismol. Soc. Am. 103, 2025–2046. doi:10.1785/0120120328

Veloza, G., Styron, R., Taylor, M., Mora, A., 2012. Open-source archive of active faults for northwest South America. GSA Today 22, 4–10. doi:10.1130/GSAT-G156A.1

Villagómez, D., Spikings, R., 2013. Thermochronology and tectonics of the Central and Western Cordilleras of Colombia: Early Cretaceous-Tertiary evolution of the Northern Andes. Lithos 160–161, 228–249. doi:10.1016/j.lithos.2012.12.008

Villagómez, D., Spikings, R., Magna, T., Kammer, A., Winklerd, W., Beltrán, A., 2011. Geochronology, geochemistry and tectonic evolution of the Western and Central cordilleras of Colombia. Lithos 125, 875–896. doi:10.1016/j.lithos.2011.05.003

Villamizar-Escalante, N., Bernet, M., Urueña-Suárez, C., Hernández-González, J.S.S., Terraza-Melo, R., Roncancio, J., Muñoz-Rocha, J.A.A., Peña-Urueña, M.L.L., Amaya, S., Piraquive, A., 2021. Thermal history of the southern Central Cordillera and its exhumation record in the Cenozoic deposits of the Upper Magdalena Valley, Colombia. J. South Am. Earth Sci. 107, 103105. doi:10.1016/j.jsames.2020.103105

von Humboldt, A., Bonpland, A., 2013. Essay on the geography of plants. The University of Chicago Press. doi:10.14237/ebl.4.2013.19

Wagner, L.S., Jaramillo, J.S., Ramírez-Hoyos, L.F., Monsalve, G., Cardona, A., Becker, T.W., 2017. Transient slab flattening beneath Colombia. Geophys. Res. Lett. 44, 6616–6623. doi:10.1002/2017GL073981

Whipple, K.X., Tucker, G.E., 1999. Dynamics of the stream-power river incision model: Implications for height limits of mountain ranges, landscape response timescales, and research needs. J. Geophys. Res. Solid Earth 104, 17661–17674. doi:10.1029/1999JB900120

Willett, S.D., McCoy, S.W., Perron, J.T., Goren, L., Chen, C.-Y., 2014. Dynamic Reorganization of River Basins. Science 343, 1248765–1248765. doi:10.1126/science.1248765

Wobus, C., Whipple, K.X., Kirby, E., Snyder, N., Johnson, J., Spyropolou, K., Crosby, B., Sheehan, D., 2006. Tectonics from topography: Procedures, promise, and pitfalls. Spec. Pap. Geol. Soc. Am. 398, 55–74. doi:10.1130/2006.2398(04)

Zapata, S., Patiño, A., Cardona, A., Parra, M., Valencia, V., Reiners, P., Oboh-Ikuenobe, F., Genezini, F., 2020. Bedrock and detrital zircon thermochronology to unravel exhumation histories of accreted tectonic blocks: An example from the Western Colombian Andes. J. South Am. Earth Sci. 103. doi:10.1016/j.jsames.2020.102715

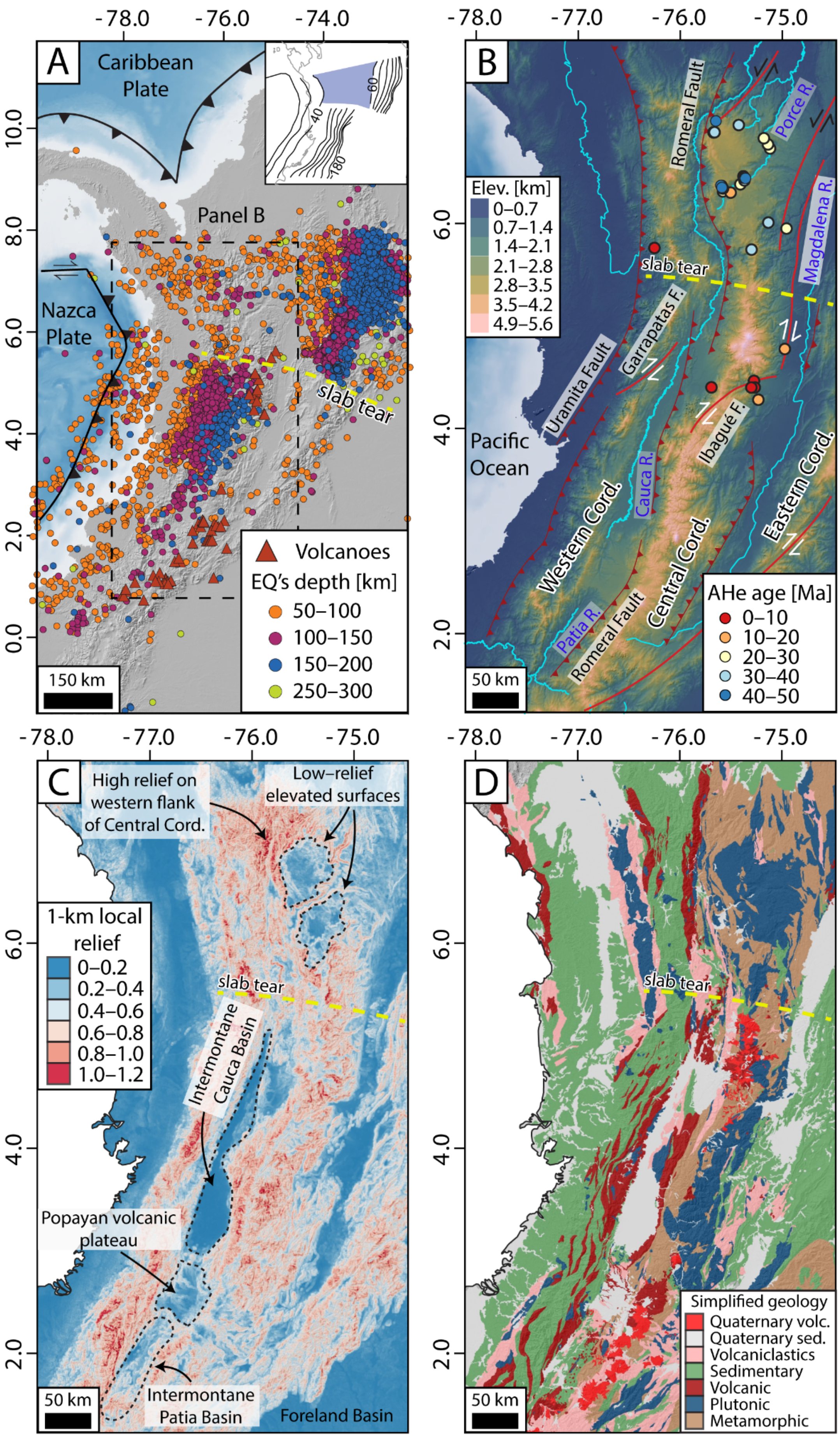

A
Caribbean Plate
Nazca Plate
Panel B
slab tear
Volcanoes
EQ's depth [km]
50–100
100–150
150–200
250–300
150 km
B
Romeral Fault
Porce R.
Magdalena R.
Elev. [km]
0–0.7
0.7–1.4
1.4–2.1
2.1–2.8
2.8–3.5
3.5–4.2
4.9–5.6
slab tear
Garrapatas F.
Uramita Fault
Pacific Ocean
Cauca R.
Ibagué F.
Eastern Cord.
Western Cord.
Central Cord.
Patia R.
Romeral Fault
AHe age [Ma]
0–10
10–20
20–30
30–40
40–50
50 km
C
High relief on western flank of Central Cord.
Low–relief elevated surfaces
1-km local relief
0–0.2
0.2–0.4
0.4–0.6
0.6–0.8
0.8–1.0
1.0–1.2
slab tear
Intermontane Cauca Basin
Popayan volcanic plateau
Intermontane Patia Basin
Foreland Basin
50 km
D
slab tear
Simplified geology
Quaternary volc.
Quaternary sed.
Volcaniclastics
Sedimentary
Volcanic
Plutonic
Metamorphic
50 km

Fig. 1. Study area overview. A. Shaded relief showing the spatial distribution of volcanoes and earthquake hypocenters deeper than 50 km. Box highlights the extent of panels (B) to (D). Inset: slab depth contours from Wagner et al. 2017, with blue shading highlighting the flat slab. B. Topography of the Western and Central Cordilleras and main geological structures (modified from Veloza et al., 2012), as well as compiled apatite (U-Th)/He (AHe) thermochronology ages (Villagomez and Spikings, 2013; Restrepo-Moreno et al., 2009). C. Local relief calculated with a 1–km radius. D. Simplified lithologic map of the Northern Andes (modified from Gomez et al., 2015).

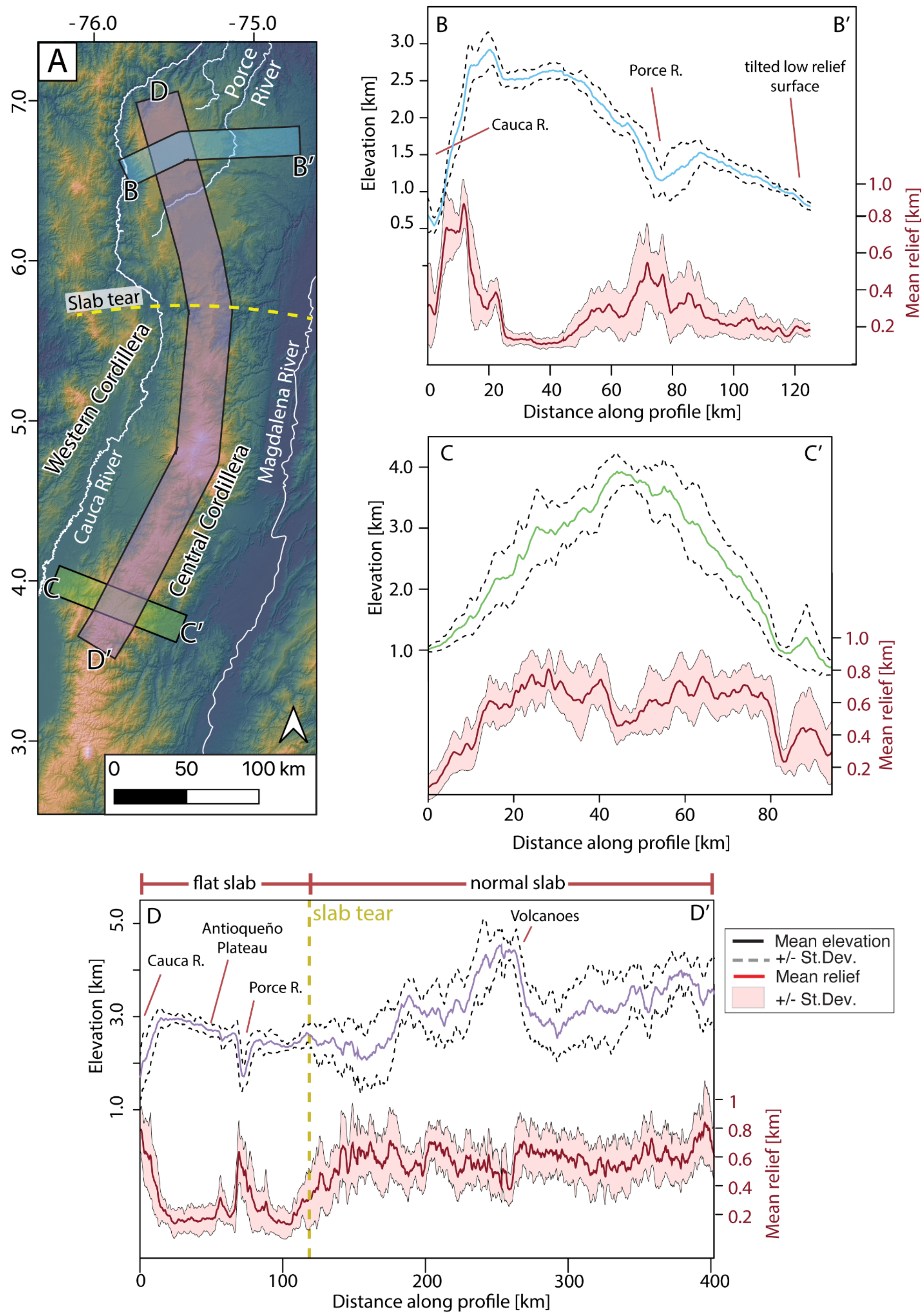
A
-76.0
-75.0
7.0
6.0
5.0
4.0
3.0
D
B
B′
C
C′
D′
Porce River
Slab tear
Western Cordillera
Cauca River
Central Cordillera
Magdalena River
0 50 100 km
B
B′
Elevation [km]
Mean relief [km]
Cauca R.
Porce R.
tilted low relief surface
Distance along profile [km]
C
C′
Elevation [km]
Mean relief [km]
Distance along profile [km]
flat slab
normal slab
slab tear
D
D′
Cauca R.
Antioqueño Plateau
Porce R.
Volcanoes
Elevation [km]
Mean relief [km]
Distance along profile [km]
Mean elevation
+/- St.Dev.
Mean relief
+/- St.Dev.

Fig. 2. Along strike variations in the topography and local relief (1-km radius) of the Central Cordillera. A. Topography of the Central Cordillera with the location of the swath profiles B–D.

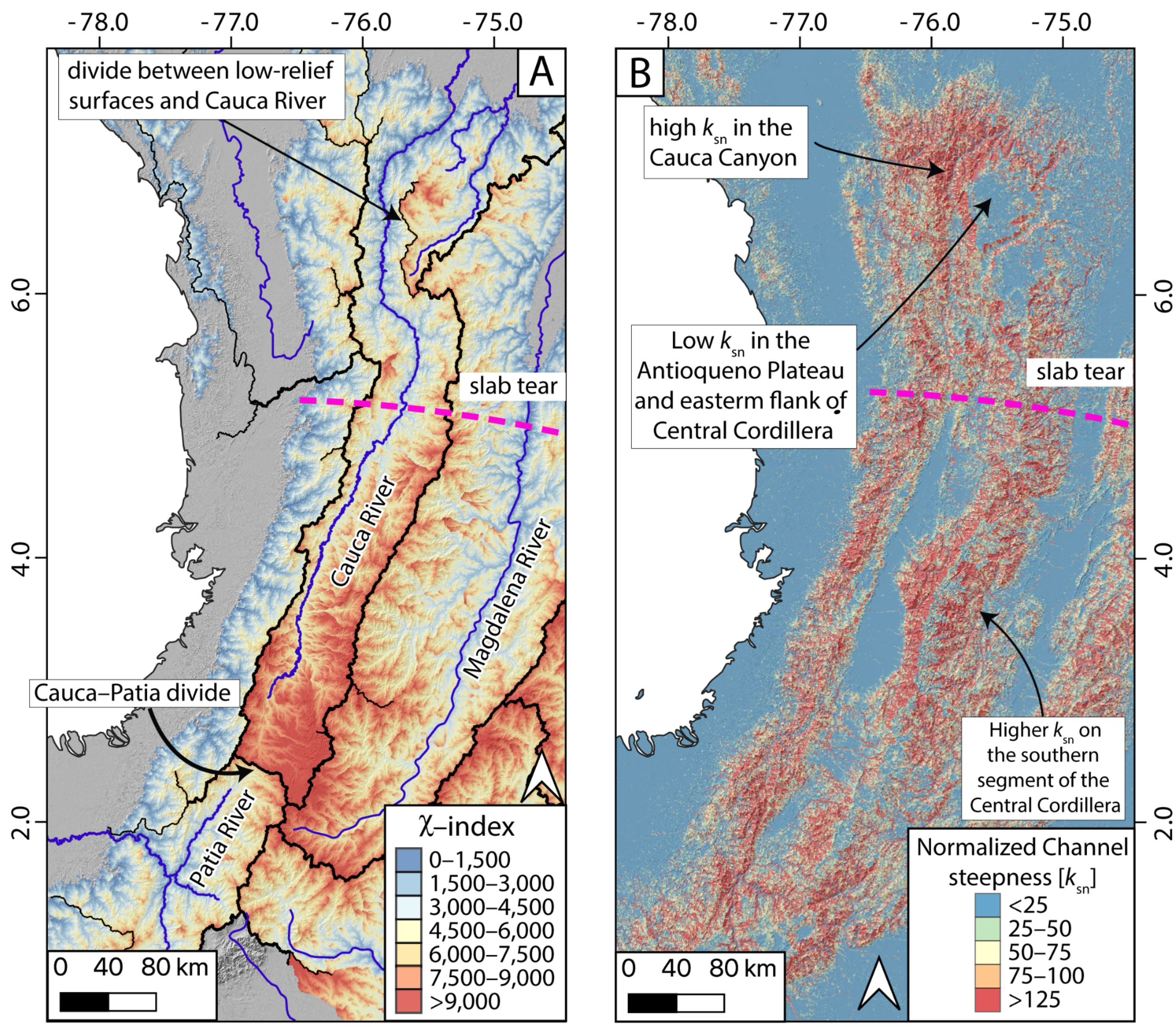

Fig. 3. River network metrics. A. χ–map of the Western and Central Cordillera. B. Map of normalized channel steepness index (k_{sn}).

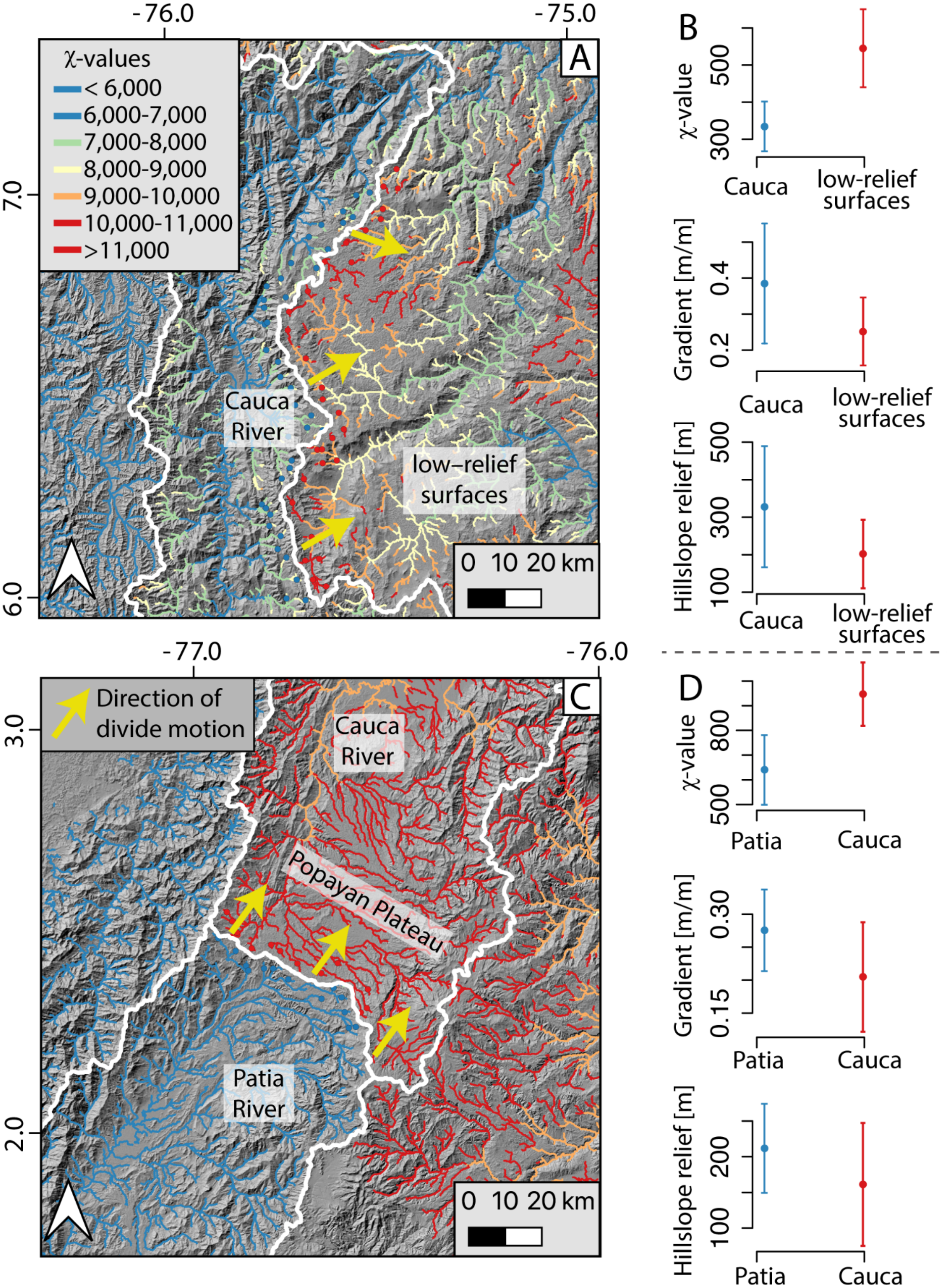

-76.0
-75.0
7.0
6.0
A
χ-values
< 6,000
6,000-7,000
7,000-8,000
8,000-9,000
9,000-10,000
10,000-11,000
>11,000
Cauca River
low–relief surfaces
0 10 20 km
B
χ-value
300
500
Cauca
low-relief surfaces
Gradient [m/m]
0.2
0.4
Hillslope relief [m]
100
300
500
-77.0
-76.0
3.0
2.0
C
Direction of divide motion
Cauca River
Popayan Plateau
Patia River
D
500
800
Patia
Cauca
0.15
0.30
100
200

Fig. 4. Close up of prominent disequilibrium divides bordering the Cauca River basin. A. χ-map of the northern Central and Western Cordilleras. B. Median and quartile values of channel head χ, local relief (500m radius), and hillslope gradient for both sides of the divide in (A). Channel heads included in the calculation are highlighted by circles. The divide between the Cauca River and the low-relief surfaces of the Central Cordillera is predicted to migrate towards the east as indicated by the differences in χ, hillslope gradient, and local relief. C. χ-map of the southern Central and Western Cordillera and the drainage divide between the Cauca and Patía rivers. D. Same as (B) for the Cauca-Patía divide shown in (C). The topographic metrics predict divide migration towards the northeast.

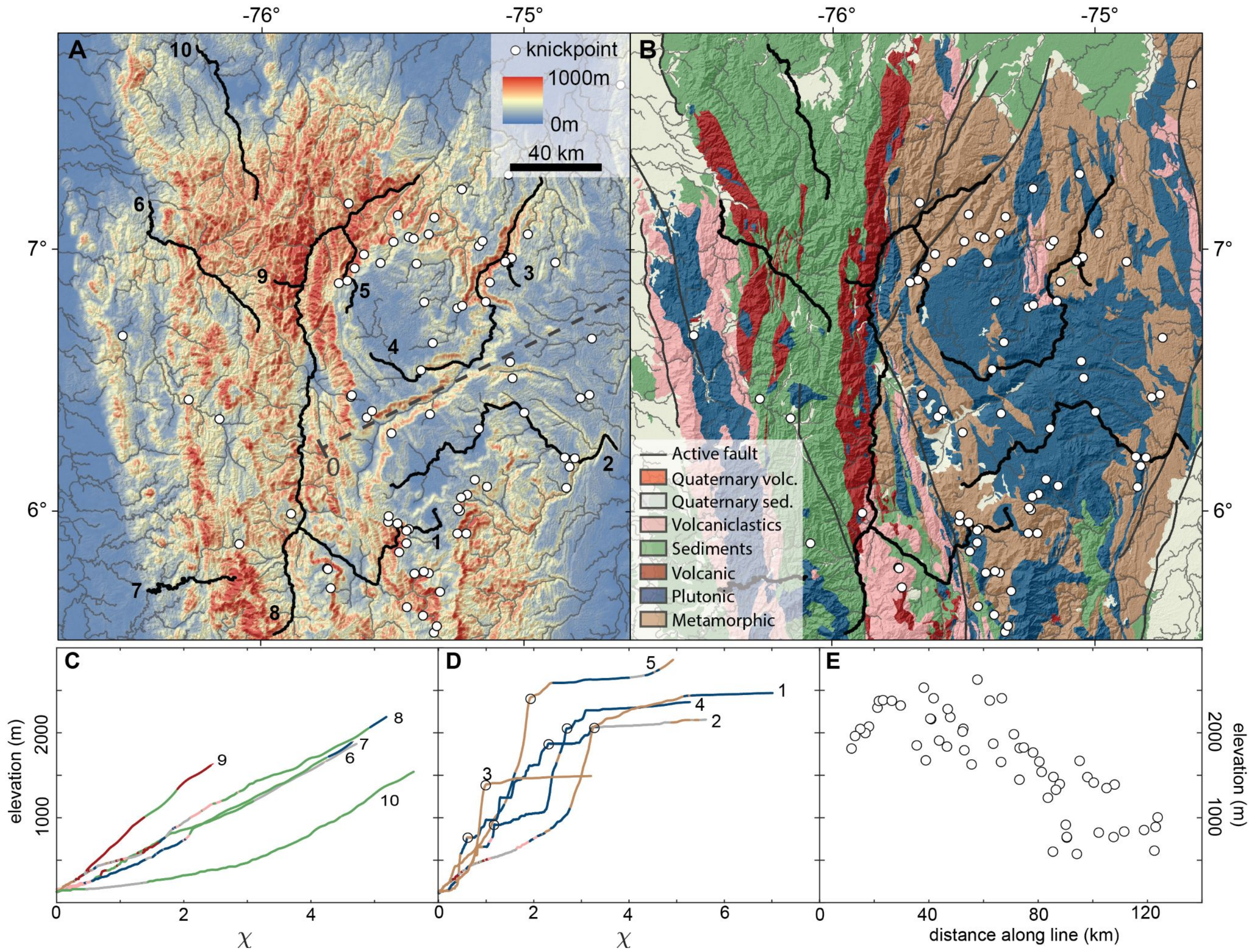

Fig. 5. χ profiles and knickpoints in the northern Central and Western Cordillera (Antioqueño Plateau area). A. Local relief map with knickpoint locations (white points) and stream network (black lines). B. Simplified geologic map with active faults and the location of knickpoints. Note that knickpoints do not align with lithologic boundaries nor active faults. C. Representative χ-profiles of the northern segment of the Western Cordillera colored by lithology according to (B). The streams are highlighted in (A). Most rivers in the Western Cordillera show well graded χ-profiles indicative of equilibrium river profiles. Stream no. 10 highlights that the rivers in the northern flank of the Western Cordillera tend towards higher concavity values than the rest of the

streams. D. Representative river profiles of the Antioqueno Plateau area. E. Elevation of knickpoints projected onto the profile line indicated in (A). Note the smooth decrease in knickpoint elevations eastwards, following the slope of the low relief surfaces.

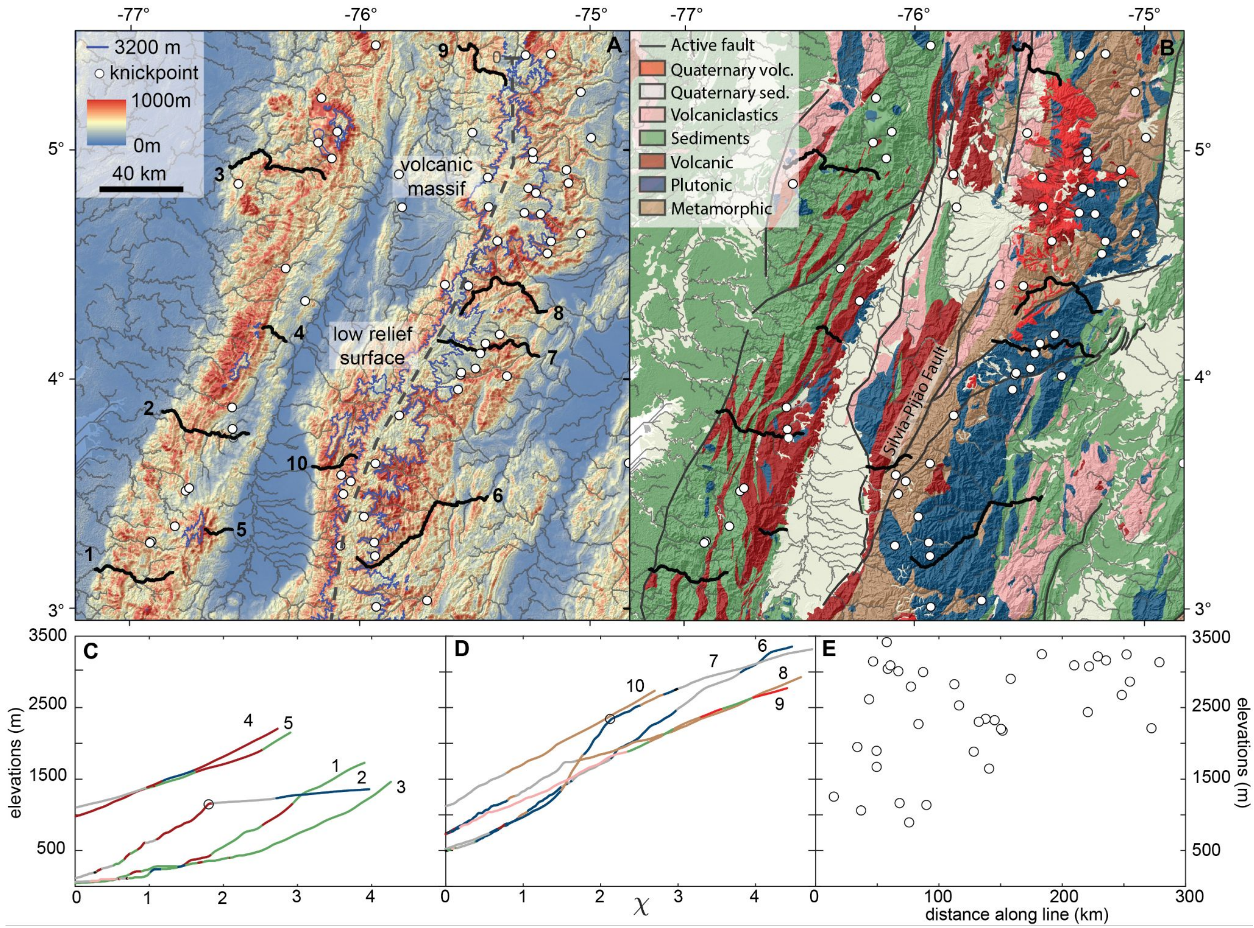

Fig. 6. χ-profiles and knickpoints in the southern segment of the Central and Western Cordillera. A. Local relief map with knickpoint locations (white points) and stream network (black lines). Blue line indicates the 3,200m elevation contour related to the extent of glacial moraines. B. Simplified geologic map with active faults and the location of knickpoints. C. Representative χ-profiles of the southern Western Cordillera. Most rivers in the Western Cordillera are in equilibrium. D. Representative χ-profiles of the southern Central Cordillera colored by lithology according to Fig. 1D. Stream no. 7 traverses the low relief surfaces south of the city of Ibagué. E. Elevation of knickpoints projected onto the profile line indicated in (A).

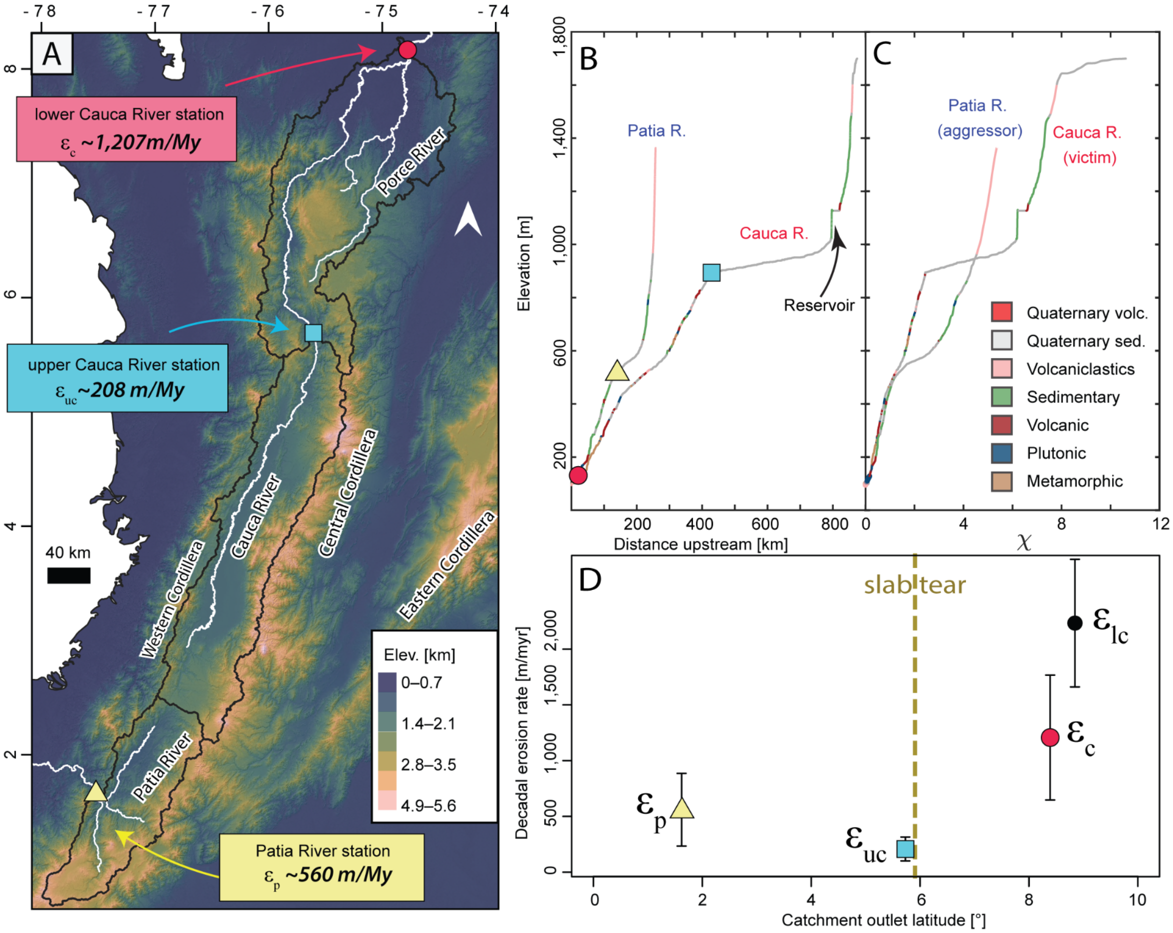

Fig. 7. Comparison of river profiles and erosion rates in the Patía and Cauca rivers. A. Location of the rivers and gauge stations used to calculate erosion rates B. Elevation profiles of the Cauca and Patía Rivers C. χ-profiles of the Cauca and Patía Rivers. D. Decadal erosion rates values for the gauge stations displayed in C.

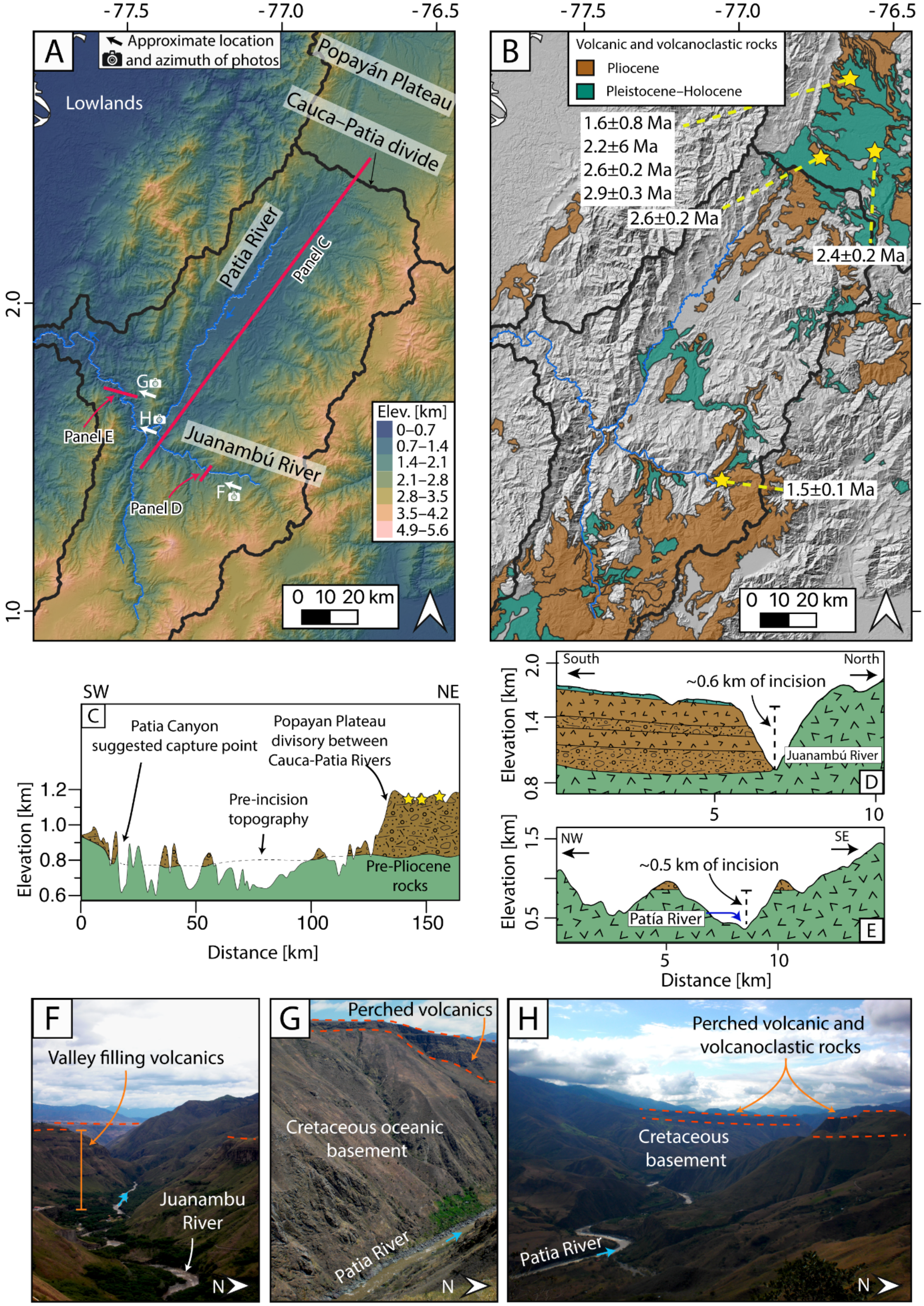
A
Approximate location and azimuth of photos
Popayán Plateau
Cauca–Patia divide
Lowlands
Patia River
Panel C
Panel E
Panel D
Juanambú River
Elev. [km]
0–0.7
0.7–1.4
1.4–2.1
2.1–2.8
2.8–3.5
3.5–4.2
4.9–5.6
0 10 20 km
B
Volcanic and volcanoclastic rocks
Pliocene
Pleistocene–Holocene
1.6±0.8 Ma
2.2±6 Ma
2.6±0.2 Ma
2.9±0.3 Ma
2.6±0.2 Ma
2.4±0.2 Ma
1.5±0.1 Ma
C
SW
NE
Patia Canyon suggested capture point
Popayan Plateau divisory between Cauca-Patia Rivers
Pre-incision topography
Pre-Pliocene rocks
Elevation [km]
Distance [km]
D
South
North
~0.6 km of incision
Juanambú River
E
NW
SE
~0.5 km of incision
Patía River
F
Valley filling volcanics
Juanambu River
G
Perched volcanics
Cretaceous oceanic basement
Patia River
H
Perched volcanic and volcanoclastic rocks
Cretaceous basement
Patia River

Fig. 8. Evidence of volcanic filling and subsequent incision in the Patía River catchment. A. Topography of the Patía River Basin labeled with main topographic features. Red lines indicate the location of the cross sections displayed in C–E. B. Hillshade with the location of Pliocene to Holocene volcanic rocks. Yellow stars highlight the locations of geochronology ages (Table S2). C. Approximately N–S cross section across the Patía Basin showing the location and elevation of the Popayan Plateau and the valley filling volcanic deposits, now perched above the modern rivers. D. Cross section of the Juanambú River Canyon. E. Cross section of the Patía Canyon, where the river crosses the Western Cordillera F. View to the west of the Juanambú Canyon showing flat-lying valley-filling volcanics on the left. G–H. Views of the western wall of the Patía Canyon. Perched volcanic deposits can be seen unconformably overlying the Cretaceous oceanic basement of the Western Cordillera.

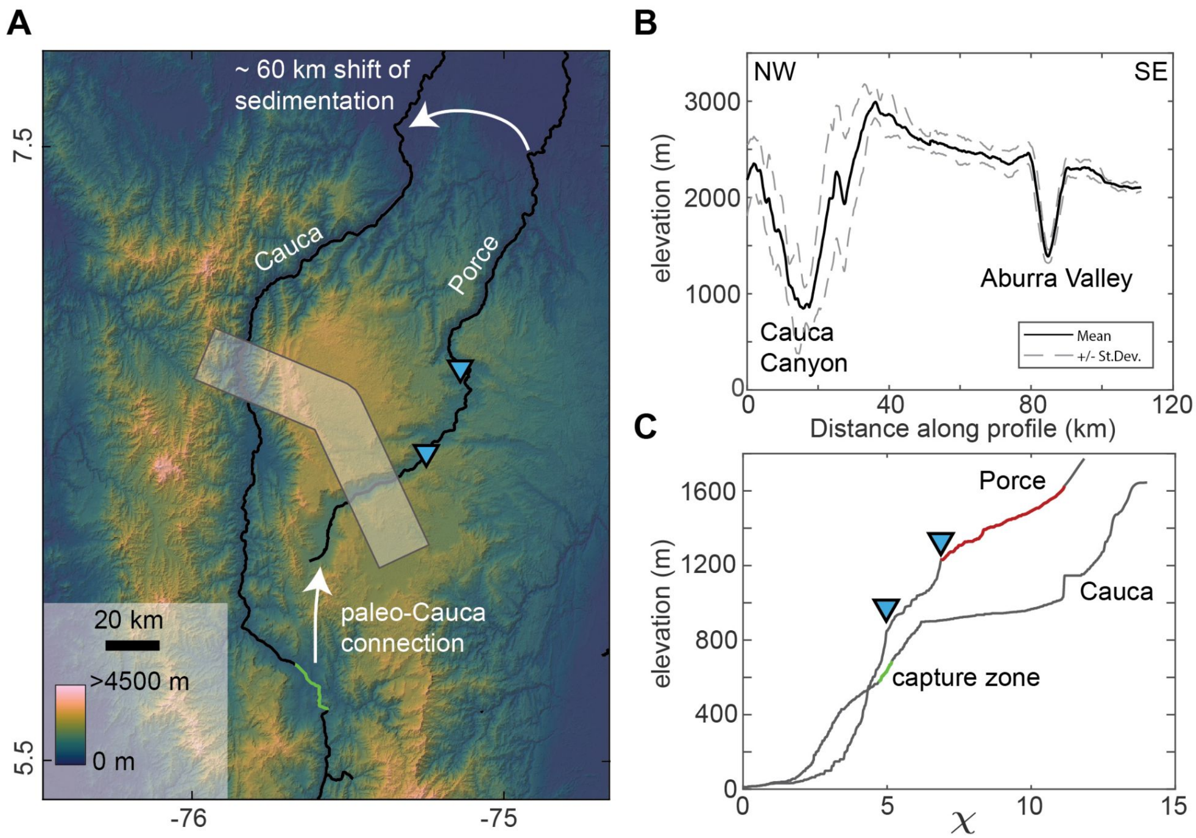

Fig. 9. Cauca–Porce capture hypothesis. A. Location of proposed capture and paleo-Cauca flow path. Blue triangles mark the locations of knickpoints in the Porce River profile in panel C. The white box indicates the location of the swath profile and the green river segment indicates the estimated capture zone. Note the abrupt end of the deeply incised Porce River canyon, suggesting a missing headwater area. B. Swath profile across the Cauca Canyon and Porce River Canyon (Aburra Valley). C. χ vs. elevation profiles of the Cauca and Porce rivers. Red line indicates the portion of the Porce River profile that could correspond to the approximate pre-capture paleo-Cauca profile.

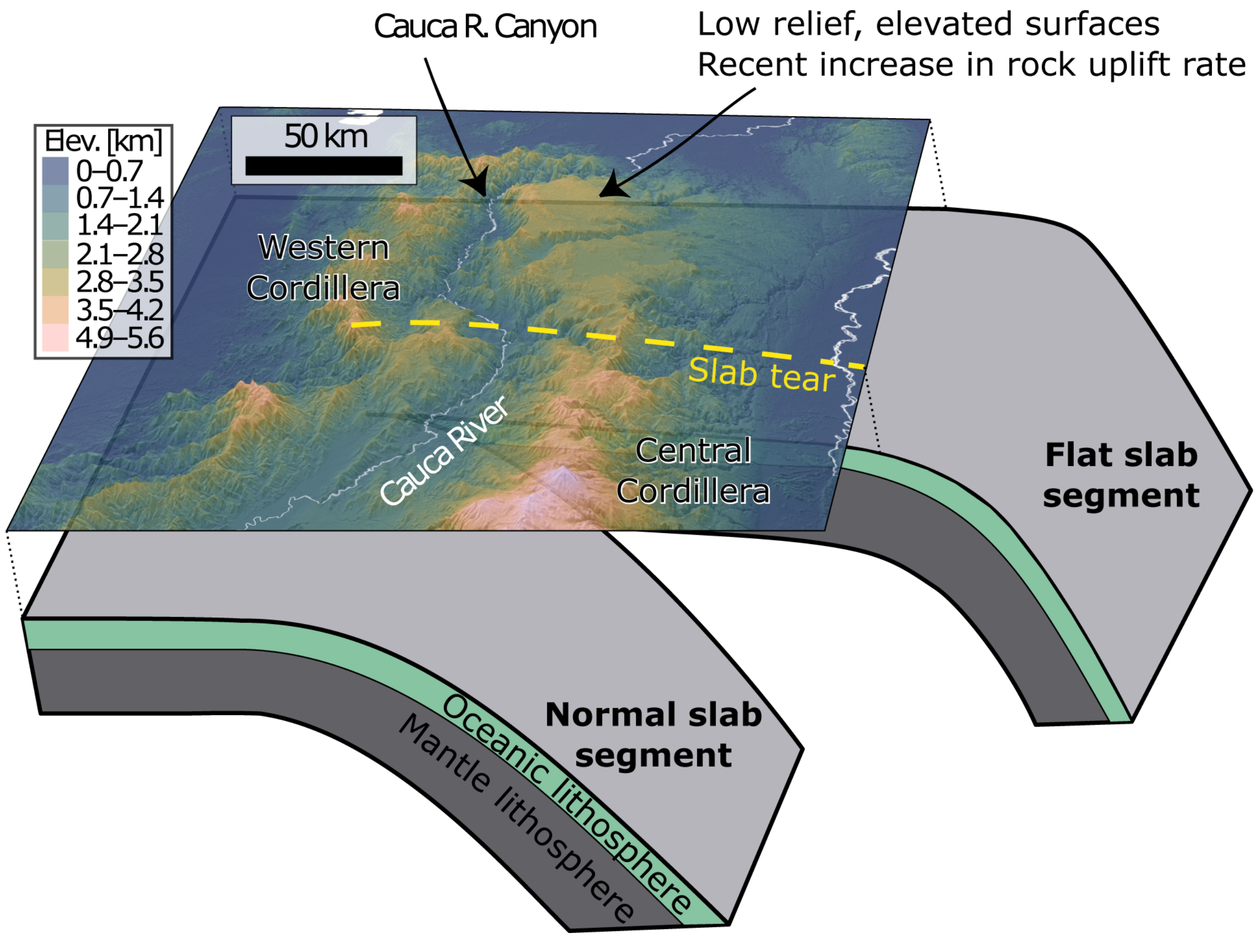

Fig. 10. Topographic response of the Western and Central cordilleras to variations in slab geometry. The upper plate lithosphere is not displayed for better visualization of the subducting slab geometries.

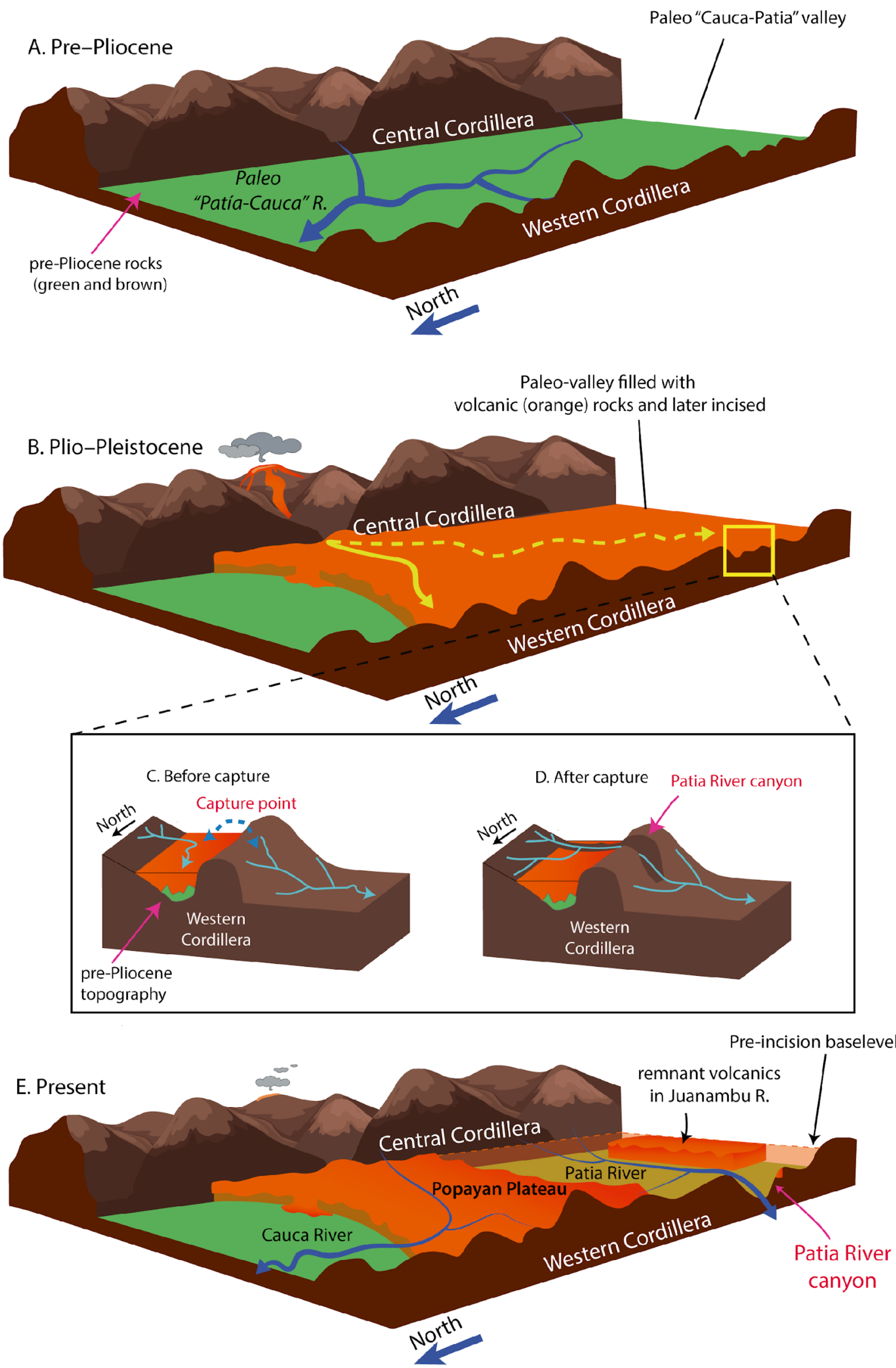

A. Pre–Pliocene
Paleo "Cauca-Patia" valley
Central Cordillera
Paleo
"Patía-Cauca" R.
Western Cordillera
pre-Pliocene rocks
(green and brown)
North
B. Plio–Pleistocene
Paleo-valley filled with
volcanic (orange) rocks and later incised
Central Cordillera
Western Cordillera
North
C. Before capture
Capture point
North
Western
Cordillera
pre-Pliocene
topography
D. After capture
Patia River canyon
North
Western
Cordillera
E. Present
Pre-incision baselevel
remnant volcanics
in Juanambu R.
Central Cordillera
Patia River
Popayan Plateau
Cauca River
Western Cordillera
Patia River
canyon
North

1080

Fig. 10. Schematic hypothesis for the evolution of the Patía Basin. A. Schematic view of the pre-Pliocene paleo "Cauca–Patía" valley when the basins were connected and occupied by a north flowing paleo-Cauca-Patia river. B. Deposition of large volumes of volcanic and volcaniclastic rocks in the Pliocene and Pleistocene sourced from volcanic edifices in the Central Cordillera, especially in the area of the Popayan Plateau. C-D. Schematic hypothesis of the capture of the Patía Basin via spillover as a result of the increase in base level following the emplacement of the volcanic deposits. E. Schematic view of the volcanic Popayan Plateau forming the topographic divide between the Cauca and Patía rivers. Notice how the level of volcanic deposits extended towards the Patía Basin.

Supplementary Materials

This supporting information contains three figures (Figures S1 to SXX) and one table (Table S1) that are cited in the main manuscript.

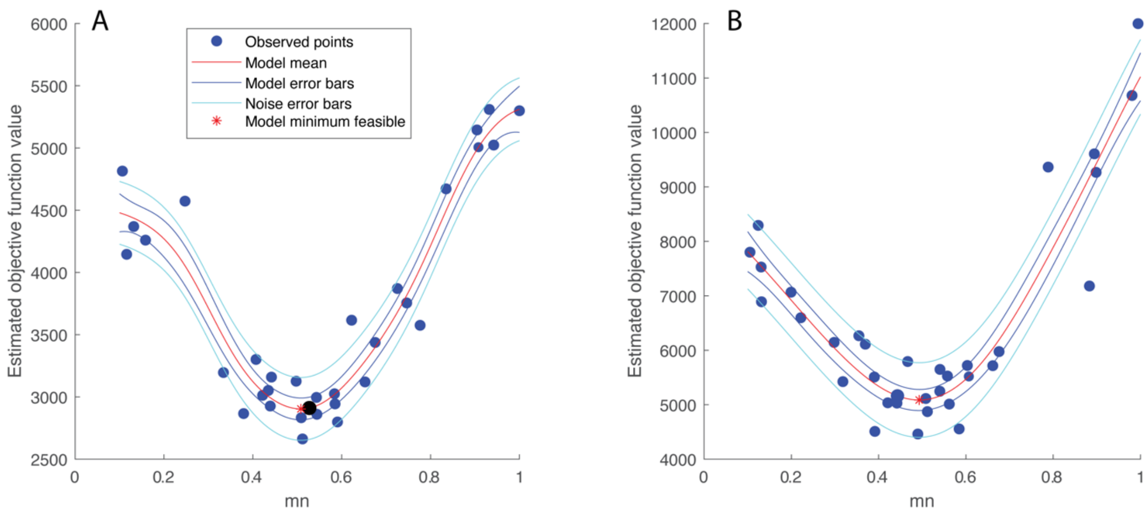

Figure S1. Estimates of best-fit concavity for the rivers of the Western Cordillera (panel A) and Central Cordillera (panel B).

Climate

In the Western and Central Cordilleras of Colombia, moisture is transported from the Pacific Ocean by the low-level (i.e., low elevation) westerly winds of the Choco Jet and from the Atlantic Ocean by high-level easterly (trade) winds. The western side of the Western Cordillera forms a strong orographic barrier where precipitation is focused, making it one of Earth's rainiest locations with precipitation rates of 8–13 m/yr (e.g., Poveda and Mesa, 2000). The eastern flank of the Western Cordillera and the intermontane valleys between the Western and Central Cordilleras only receive ~2–3 m/yr of precipitation (Figure S1).

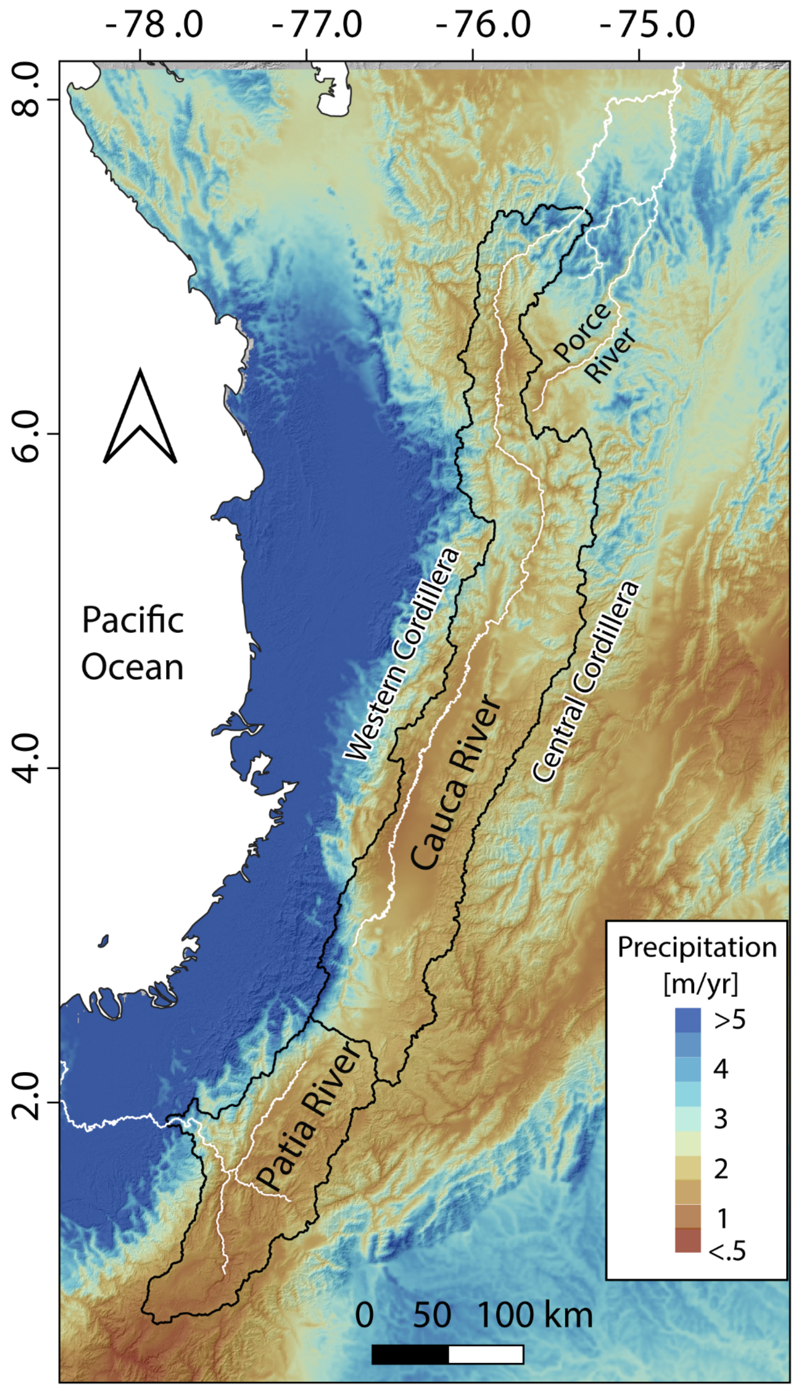

Figure S2. Precipitation map of the Northern Andes. Data derived from the CHELSA (Karger et al., 2017) dataset.

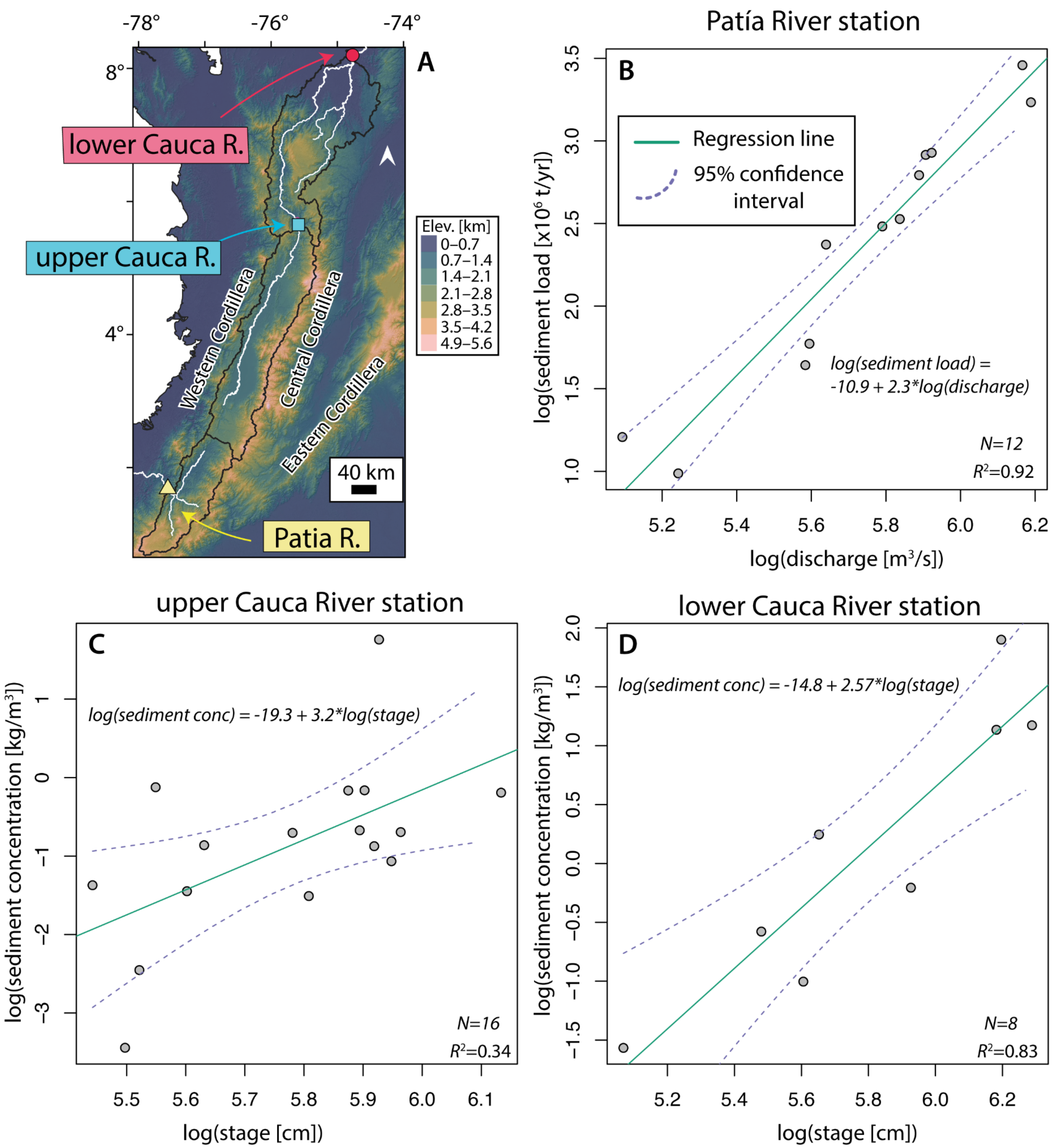

Figure S3. Rating curves for the Cauca and Patia Rivers. A. Location of the gauge stations. B-D. Power law fits of sediment load vs stage or water discharge.

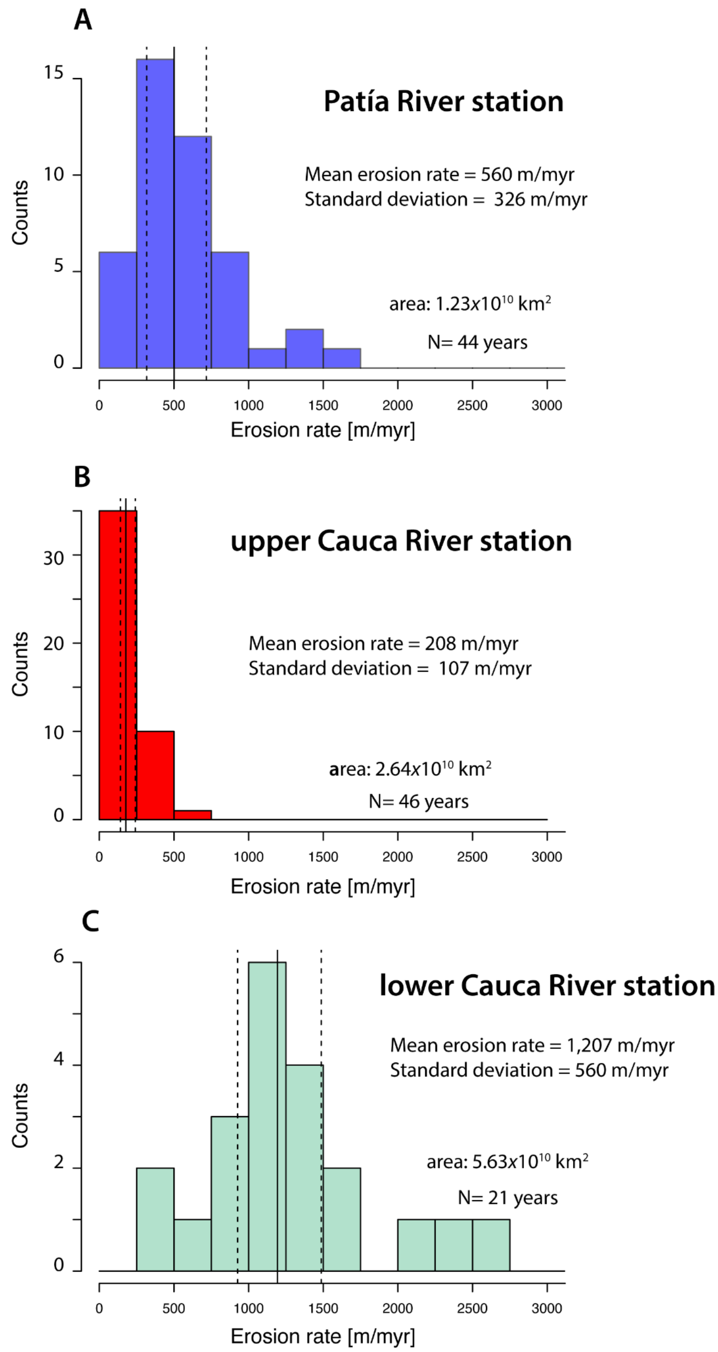

Figure S4. Distribution of estimated annual erosion rate values (A-C). The erosion rate values were predicted using the power-law fits from figure S3. The reported statistics and uncertainties correspond to the mean and standard deviation of the annual erosion rate distribution.

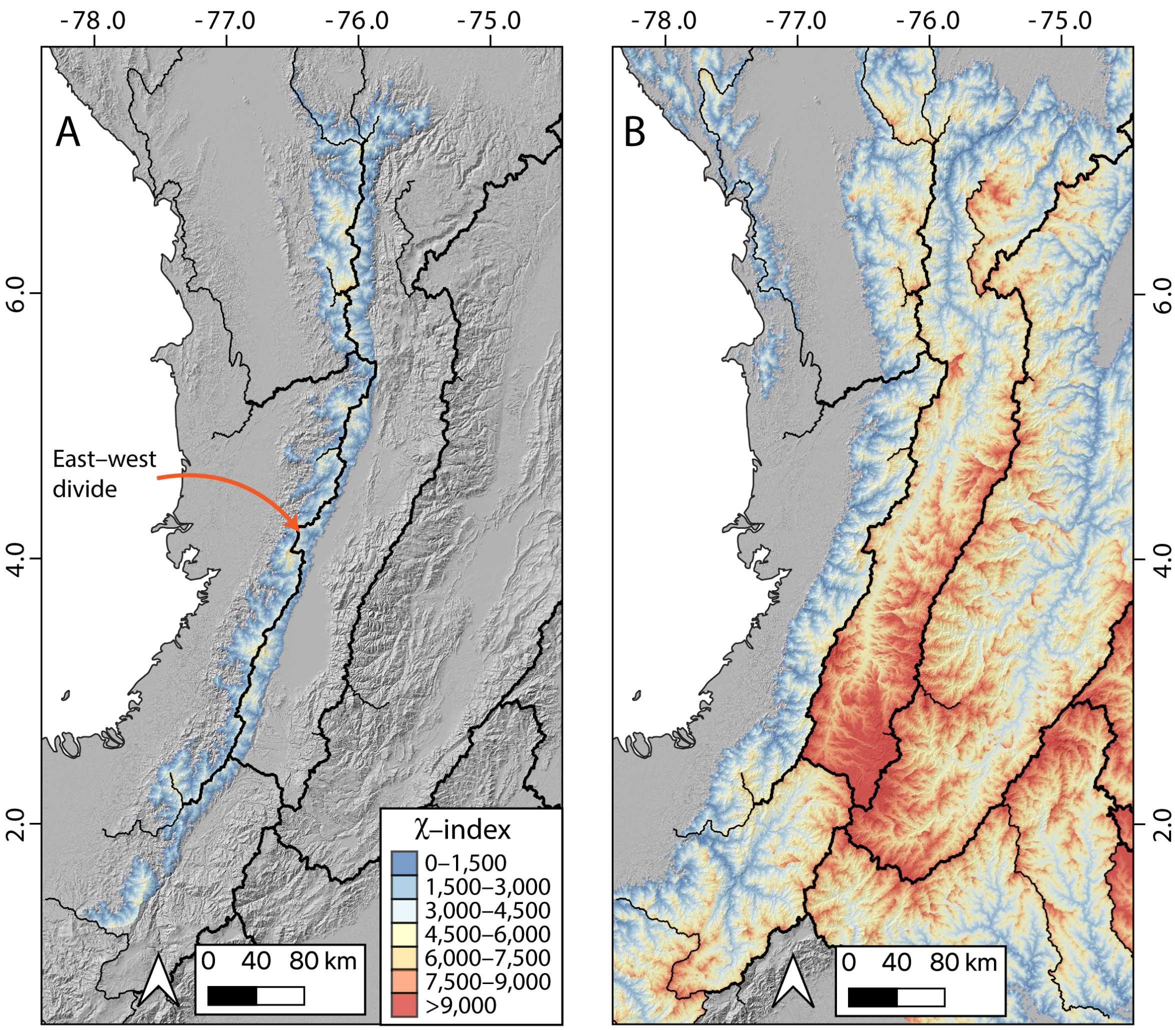

Figure S5. Effect of baselevel on χ. A. χ–map of the Western Cordillera using a baselevel of 950m. B. χ–map of the Northern Andes using a baselevel of 200m. Note that when using the 950 m baselevel the east–west drainage divide across the Western Cordillera does not show any major difference in χ.

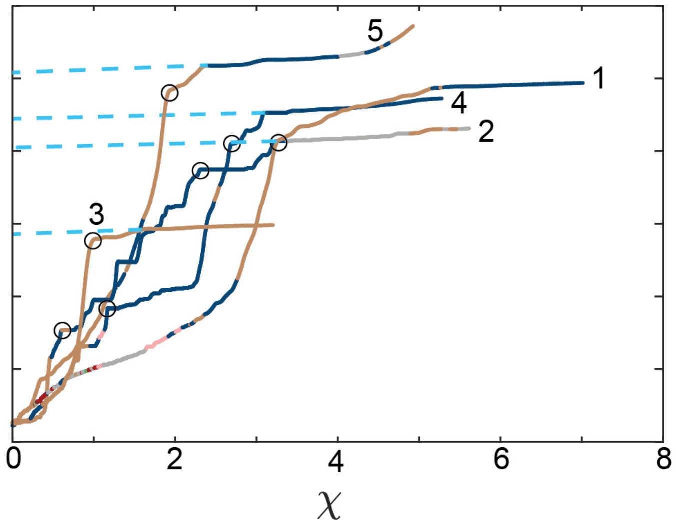

Figure S6. River profiles from the top of the Antioqueno Plateau projected to the baselevel of integration. This is an estimate of the channel geometry before the onset of increased uplift. The difference between the upstream end of the profile and the downstream end of the projected profile constrains the total amount of fluvial relief within the landscape, which amounts to ~ 200 m. Together with the 250 m of baselevel elevation, this estimate predicts that fluvial channels in the region of the Antioqueno Plateau initiated at ~ 450m above sea level elevation prior to the increased uplift.

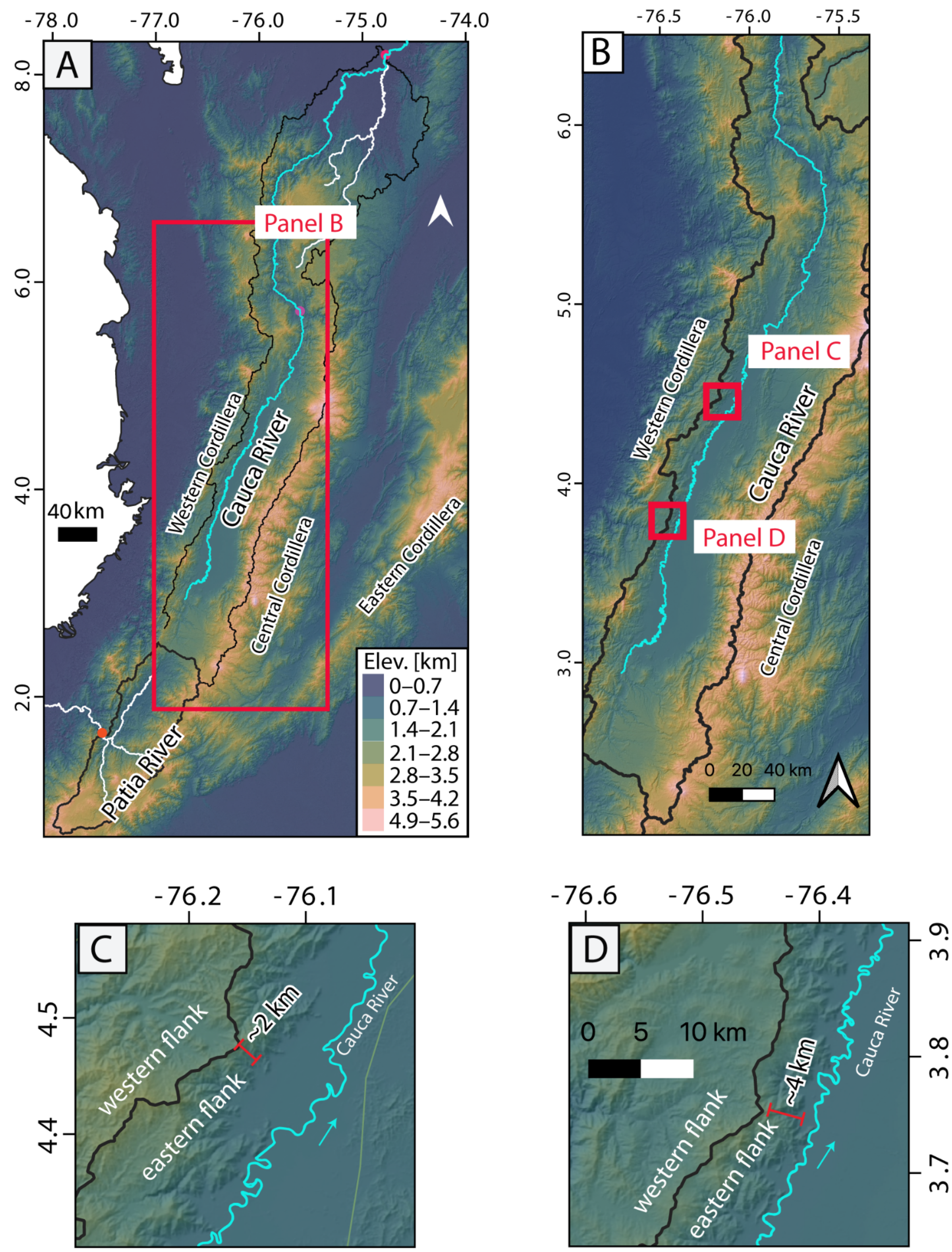

Figure S7. Close up to the topography of the Cauca Basin. Note the two locations where the distance between the east–west drainage divide and the Cauca River is <5 km. The proximity of the drainage divide to the Cauca River could lead to drainage capture of the upper Cauca Basin by a west draining tributary. A-B. Index maps. B-C. Close ups of the topography.

Table S1. IDEAM gauge station information.

IDEAM Station Code	Station name	Lat.	Long.	River	Drainage area [x1010 km2]	No. of sediment load observations	No. of water discharge measurements
26187110	La Pintada	5.73	-75.61	upper Cauca R.	2.63	16 [1998-2014]	18,870 [1968-2021]
25027200	Las Varas	8.39	-74.56	lower Cauca R.	5.63	8 [1998-2014]	7,307 [1988-2008]
52077010	Puente Pusmeo	1.62	-77.48	Patia R.	1.23	12 [1972-1993]	15,120 [1968-2021]

Table S2. Compiled ages of the volcanic rocks in the Patía Basin.

Sample	Lat	Lon	Age	Error	Method	References	Comment
PKSW-087c	2.48	-76.74	2.56	0.24	Ar-Ar	Torres (2010)	
PKSW-043a	2.76	-76.69	2.2	6.3	Ar-Ar	Torres (2010)	
PKSW-043b	2.76	-76.69	1.6	0.8	Ar-Ar	Torres (2010)	
PKSW-080a	2.76	-76.69	2.62	0.21	Ar-Ar	Torres (2010)	
PKSW-037a	2.76	-76.69	2.88	0.26	Ar-Ar	Torres (2010)	
27	2.45	-76.59	2.4	0.2	K-Ar	Risnes (1995)	
2	1.44	-77.05	1.5	0.1	K-Ar	Murcia and Pichler (1986)	Approximate location based on descriptions in paper